Meteorologische Zeitschrift, PrePub DOI 10.1127/metz/2016/0776

Radiative forcing from aircraft emissions of NO_x: model calculations with CH_4 surface flux boundary condition

Giovanni Pitari[1]*, Irene Cionni[2], Glauco Di Genova[1], Ole Amund Søvde[3] and Ling Lim[4]

[1]Department of Physical and Chemical Sciences, Università dell'Aquila, L'Aquila, Italy
[2]Enea, Ente per le Nuove Tecnologie, l'Energia e l'Ambiente, Roma, Italy
[3]Center for International Climate and Environmental Research – Oslo (CICERO), Norway
[4]Faculty of Science and Engineering, Manchester Metropolitan University, Manchester, UK;

(Manuscript received January 15, 2016; in revised form June 30, 2016; accepted September 16, 2016)

Abstract

Two independent chemistry-transport models with troposphere-stratosphere coupling are used to quantify the different components of the radiative forcing (RF) from aircraft emissions of NO_x, *i.e.*, the University of L'Aquila climate-chemistry model (ULAQ-CCM) and the University of Oslo chemistry-transport model (Oslo-CTM3). The tropospheric NO_x enhancement due to aircraft emissions produces a short-term O_3 increase with a positive RF (+17.3 mW/m^2) (as an average value of the two models). This is partly compensated by the CH_4 decrease due to the OH enhancement (−9.4 mW/m^2). The latter is a long-term response calculated using a surface CH_4 flux boundary condition (FBC), with at least 50 years needed for the atmospheric CH_4 to reach steady state. The radiative balance is also affected by the decreasing amount of CO_2 produced at the end of the CH_4 oxidation chain: an average CO_2 accumulation change of −2.2 ppbv/yr is calculated on a 50 year time horizon (−1.6 mW/m^2). The aviation perturbed amount of CH_4 induces a long-term response of tropospheric O_3 mostly due to less HO_2 and CH_3O_2 being available for O_3 production, compared with the reference case where a constant CH_4 surface mixing ratio boundary condition is used (MBC) (−3.9 mW/m^2). The CH_4 decrease induces a long-term response of stratospheric H_2O (−1.4 mW/m^2). The latter finally perturbs HO_x and NO_x in the stratosphere, with a more efficient NO_x cycle for mid-stratospheric O_3 depletion and a decreased O_3 production from HO_2+NO in the lower stratosphere. This produces a long-term stratospheric O_3 loss, with a negative RF (−1.2 mW/m^2), compared with the CH_4 MBC case. Other contributions to the net NO_x RF are those due to NO_2 absorption of UV-A and aerosol perturbations (the latter calculated only in the ULAQ-CCM). These comprise: increasing sulfate due to more efficient oxidation of SO_2, increasing inorganic and organic nitrates and the net aerosols indirect effect on warm clouds. According to these model calculations, aviation NO_x emissions for 2006 produced globally a net cooling effect of −5.7 mW/m^2 (−6.2 and −5.1 mW/m^2, from ULAQ and Oslo models, respectively). When the effects of aviation sulfur emissions are taken into account in the atmospheric NO_x balance (via heterogeneous chemistry), the model-average net cooling effects of aviation NO_x increases to −6.2 mW/m^2. Our study applies to a sustained and constant aviation NO_x emission and for the given background NO_y conditions. The perturbation picture, however, may look different if an increasing trend in aviation NO_x emissions would be allowed.

Keywords: Aviation NO_x, Long-term aviation effects, Methane lifetime, Stratospheric water vapor, Stratospheric ozone, Tropospheric ozone

Key points: Short- and long-term global radiative effects of aviation NO_x tend to balance. CH_4 mass burden changes due to the aviation NO_x need to be explicitly calculated. Accurate radiative transfer calculations are required for the CH_4 forcing. Impacts of stratospheric H_2O and primary mode ozone are explicitly calculated. Long-term changes of stratospheric HO_x, NO_x, and O_3 are explicitly calculated.

1 Introduction

Kerosene is the main fuel used in civil aviation and its combustion primarily produces carbon dioxide (CO_2) and water vapor (H_2O). Other trace species such as nitric oxide (NO), nitrogen dioxide (NO_2), sulfur dioxide (SO_2), carbon monoxide (CO), hydrocarbons (HCs) and soot, are also emitted during the combustion process. These aircraft emissions can directly alter global atmospheric composition through CO_2, H_2O, NO_x, SO_2 and soot emissions, or indirectly by increasing tropospheric ozone (O_3) and hydroxyl radical (OH) through nitrogen oxides (NO_x) emissions, or indirectly by changing upper tropospheric cirrus cloudiness through contrails, contrail-cirrus and soot-cirrus formation. The resulting atmospheric perturbations may act on very different time scales, inducing long-term responses with CO_2 accumulation and methane (CH_4) lifetime changes or producing short-term climate responses with additional O_3 produc-

*Corresponding author: Giovanni Pitari, Università degli Studi dell'Aquila, Dipartimento di Scienze Fisiche e Chimiche, Via Vetoio, 67100 Coppito, L'Aquila, Italy; email: gianni.pitari@aquila.infn.it

tion and by increasing aerosols and cloud particles (Lee et al., 2010).

Aircraft NO_x emissions play a key role in tropospheric and lower stratospheric chemistry, by enhancing O_3 production and OH concentration (Köhler et al., 2008; Hoor et al., 2009). The chemical reaction with OH, in turn, acts as the main sink for atmospheric CH_4, so that aircraft NO_x emissions will decrease CH_4 lifetime. The lowering of CH_4 atmospheric abundance induces a cooling that may partially compensate the warming due to other aircraft gaseous impacts such as CO_2 and H_2O, as well as the warming due to upper tropospheric particle formation and aviation-induced cloudiness (Holmes et al., 2011). Temporally, the aircraft impact on O_3 is particularly complex, due to a superposition of short- and long-term effects that takes place via direct NO_x emissions (short-term) and via OH-driven CH_4 changes that can feedback on HO_x chemistry and finally on O_3 (long-term) (Holmes et al., 2011). In addition, the dilution of aircraft plumes increases the complexity of this problem; Kraabøl et al. (2002) found $\sim 20\,\%$ reduction in O_3-changes caused by aircraft NO_x while Cariolle et al. (2009) found the reduction to be in the range of 10–25 %.

The general effects of aviation NO_x have been widely discussed in the modeling community, e.g., by Köhler et al. (2008), Hoor et al. (2009), Grewe et al. (2010), Holmes et al. (2011), Köhler et al. (2012), Gottschaldt et al. (2013), providing insights to many relevant aspects of the problem (photochemistry, sensitivity approach, climate impacts, uncertainties) including recent modeling studies that focused on NO_x/aerosol interaction (Unger, 2011; Pitari et al., 2015). However, there are still knowledge gaps on the effects of aviation NO_x emissions on CH_4 lifetime and its subsequent impacts on stratospheric O_3 and H_2O concentrations. This largely stems from the computational resources available to run Chemical Transport Models (CTMs). It is computationally inexpensive for CTMs to model the effects of aviation NO_x on tropospheric O_3. This is due to its short lifetime, which is in the order of weeks, where steady state condition can be achieved from a few years of model run using constant emissions. However, CH_4 changes due to aviation NO_x emissions require more than a few CTM simulation years, since it takes CH_4 decades to reach equilibrium from perturbed OH fields (Skowron, 2013; Khodayari et al., 2015). To save computing time, the aviation community has adopted the feedback factor of 1.4 to the CH_4 lifetime change, which is applied to a reference CH_4 concentration (typically generated from the same CTM run that provides the 'short-term' O_3 response), in a simplified formulation to represent its steady state concentration (Prather et al., 2001; Holmes et al., 2011). The O_3 concentrations are then used explicitly in radiative transfer models (RTMs), to provide the radiative forcing (RF) estimate of short-term O_3, while a simplified expression from Ramaswamy et al. (2001) is used to determine the CH_4 RF. As a consequence of this type of CTM setup, whereby a fixed mixing ratio boundary condition is assumed, the RF from CH_4-induced long-term O_3 and stratospheric H_2O changes are determined as a function of CH_4 RF, as described in Myhre et al. (2013) for long-term O_3 and Myhre et al. (2007) for stratospheric H_2O. The issues surrounding the use of fixed mixing ratio boundary condition in CTMs have been discussed in IPCC (1999) and subsequently shown in other studies such as Skowron (2013) and Khodayari et al. (2015). The recent study by Khodayari et al. (2015) compared CH_4 concentration results from simulations using fixed mixing ratio boundary condition and flux boundary condition, where they found the simplified technique overestimated CH_4 concentrations by $\sim 9\,\%$.

The aim of this study is to provide a new insight to the evaluation of long-term O_3 and stratospheric H_2O RFs associated with CH_4 lifetime changes produced by the aviation-induced tropospheric OH perturbation (calculated as a full aviation signal perturbation from NO_x emissions). In this case, we have followed an approach that firstly, determined the steady state CH_4 concentrations through an explicit numerical experiment whereby the surface CH_4 was calculated using a flux boundary condition (similar to that conducted by Khodayari et al., 2015). This allows the OH change from aircraft NO_x emissions to produce a CH_4 lifetime change that was directly linked to CH_4 mixing ratio distribution. Secondly, these results were explicitly used in an offline RTM to determine the RFs for these perturbations without resorting to simplified RF expressions discussed previously. The experimental design for this study will be presented in Section 2, while the impact of this setup on atmospheric chemistry will be discussed in Section 3. A revised RF estimate of aviation NO_x induced changes to total O_3 (the sum of both the short- and long-term responses); CH_4 and its effects on stratospheric H_2O, all of which were explicitly calculated, will be presented in Section 4 of this paper.

2 Experimental design

A brief description of the numerical models and the aviation emissions dataset, along with the experimental setup used in this paper will be presented in the following subsections. For additional details on model features, we refer to Søvde et al. (2014) and Pitari et al. (2015).

2.1 ULAQ-CCM

For this study, the University of L'Aquila global scale climate-chemistry coupled model (ULAQ-CCM), which extends from the surface to the mesosphere (0.04 hPa), is operated in CTM mode and with offline radiative transfer calculations. From now on, we will refer to the chemistry-transport module of the CCM as the ULAQ-CTM. Dynamical data, *i.e.*, velocity stream-function and velocity potential, are provided by the background GCM

run in a reference case, with no feedbacks of aviation-induced changes. The oceanic surface temperature is assimilated from the Hadley Centre for Climatic Prediction and Research. A parameterization is included online for periodic natural forcings, *i.e.*, solar cycle and quasi-biennial oscillation, (Eyring et al., 2006; Morgenstern et al., 2010).

The ULAQ-CCM has been fully described in Pitari et al. (2002a and 2002b) and more recently in Pitari et al. (2014) and Pitari et al. (2015), with some important updates with respect to the previous version. These are: (a) increase of horizontal and vertical resolutions, now T21 with 126 log-pressure levels and approximate pressure altitude increment of 568 m; (b) inclusion of a parameterization to describe the formation of upper tropospheric cirrus cloud ice particles (Kärcher and Lohmann, 2002); (c) update to Sander et al. (2011) recommendations for cross sections of species, and the parameterization of Minschwaner et al. (1993) for the Schumann-Runge bands, which is based on fixed-temperature opacity distribution function formulation; (d) new radiative transfer code for photolysis calculations, solar heating rates and tropopause RF, which is based on a two-stream delta-Eddington approximation. In addition, a companion broadband, k-distribution longwave radiative module is used to compute radiative transfer and heating rates in the planetary infrared spectrum (Pitari et al., 2014).

The chemistry module is organized by long-lived and surface-flux species (CH_4, N_2O, CFCs, HCFCs, CO, NMVOC, NO_x) and by all medium and short-lived species grouped in the O_x, NO_y, HO_x, CHO_x, Cl_y, Br_y, SO_x, and aerosols families. The model includes the major components of stratospheric and tropospheric aerosols (sulfate, carbonaceous, soil dust, sea salt, PSCs). An evaluation example of the ULAQ model's tropospheric chemistry is given in Brunner et al. (2005); for the stratosphere it is given in Pitari et al. (2014) and Pitari et al. (2015). The adopted surface emissions of NO_x, CO and VOC are discussed in Søvde et al. (2014). The NO_x lightning source accounts for 5 Tg-N/yr and is treated according to Grewe et al. (2001).

The updated ULAQ radiative transfer module treats both solar (from Lyman-alpha up to 7 μm) and planetary infrared radiation interactions with major atmospheric optically active species, including gases, aerosols and clouds. The solar spectrum is split among 250 bins for chemical species photolysis rate calculation, solar heating rates and RF. The planetary infrared spectrum is treated by a k-distribution formulation over ten spectral bands (Chou et al., 2001) for the computation of heating rates and RF, including stratospheric temperature adjustment. The ULAQ radiative model results have been validated in the framework of inter-comparison campaigns: SPARC-CCMVal for photolysis rates (Chipperfield et al., 2014) and AeroCom for radiative fluxes (Randles et al., 2013).

2.2 Oslo CTM3

The Oslo CTM3 (Søvde et al., 2012) is a three dimensional offline CTM, spanning 60 layers between the surface and 0.1 hPa, with a horizontal resolution of T42 (approximately 2.8×2.8 degrees). The tropospheric sulfur cycle, sea salt aerosols and nitrate aerosols are included, in addition to tropospheric and stratospheric chemistry, as described by Søvde et al. (2012). In total, there are 111 species, of which 105 are transported, and for this study, the chemistry scheme has been updated to include stratospheric H_2O chemistry. Advection is carried out using the second order moments scheme (Prather et al., 2008; Søvde et al., 2012), using 3-hour forecasts generated by the Integrated Forecast System of the European Centre for Medium-Range Weather Forecasts (ECMWF), cycle 36r1. Vertical winds are calculated from continuity equation, except convective transport of tracers, where the convective upward flux from the ECMWF model is used. A 5 Tg-N/yr lightning NO_x source is adopted, using the vertical profiles of Ott et al. (2010). Boundary layer turbulent mixing is treated according to the Holtslag K-profile scheme (Holtslag et al., 1990). In this study, we use the meteorological year 2006 perpetually, keeping the meteorology the same from one year to the next, in order to quantify only the chemical impacts.

Anthropogenic emissions are taken from the EDGAR v4.2 dataset (EC-JRC/PBL, 2011), for year 2006, while natural emissions are taken from the MEGAN v2 (Guenther et al., 2006), where only the year 2000 data was available. Biomass burning emissions, for year 2006, are taken from GFEDv3.1 (van der Werf et al., 2010). However, the 2006 emissions of natural and biomass burning of CH_4, along with CH_4 soil uptake, are taken from Bousquet et al. (2011). Due to the long CH_4 lifetime, we scaled up its emissions to match model loss, allowing us to maintain the total burden of simulations with fixed boundary condition.

2.3 Aircraft emissions

The aircraft emissions used in this study were generated for the EU FP7 project REACT4C ("Reducing Emissions from Aviation by Changing Trajectories for the benefit of Climate") (see also Pitari et al., 2015). These were generated by the aviation emissions model FAST (Lee et al., 2005; Lee et al., 2009; Owen et al., 2010), which has been approved by the Modelling and Database Group (MDG) of the International Civil Aviation Organization (ICAO)'s Committee on Aviation Environmental Protection (CAEP) (ICAO, 2013). Aircraft movements from the CAEP Round 8 (CAEP/8) MDG work programme for the year 2006 were used as the basis of the emissions calculation. These were calculated using radar data from North American and European airspace, and for the rest of the world, the Official Airline Guide (OAG) schedule data. Routes were assumed to follow great circle trajectories and to correct for this

assumption, CAEP/8 empirical factors were applied to the distance and fuel consumption (ICAO/CAEP, 2009). The aircraft fleet was divided into 42 representative types, and the fuel flow for these was estimated with the PIANO aircraft performance model (Simos, 2008). FAST then used the fuel flow data to calculate NO_x emissions, which were based on the relationship between sea-level NO_x certification data and emissions at altitude (Lee et al., 2005). A 3D grid of 1×1 degrees horizontal spacing and 2,000 ft vertical spacing of NO_x, was generated by the FAST gridding utility, with the calculated total NO_x from aviation of 0.71 Tg-N/yr.

2.4 Numerical experiments setup

Six simulations were performed for this study: NO-AIRCRAFT (NA, simulation with no aircraft emissions), AIRCRAFT EMISSION (AE: simulation with only NO_x emissions) and AIRCRAFT EMISSION* (AE*: simulation with coupled NO_x and sulfuric acid ultrafine aerosol emissions). The latter experiment was included to account for the aircraft impact on surface area density (SAD) of sulfate aerosols for the heterogeneous chemical reactions relevant for NO_x (*i.e.*, hydrolysis of N_2O_5 and $BrONO_2$). These three experimental setups were performed with a version of ULAQ and Oslo models, firstly using a fixed CH_4 surface mixing ratio boundary condition (MBC), and then repeated using a surface flux boundary condition (FBC) for CH_4. After a preliminary model spin-up of 5 years, the MBC experiments were run for 10 years (2001–2010 for the ULAQ model and perpetual 2006 for Oslo-CTM3), allowing aircraft perturbation to reach a satisfactory statistical steady-state. The dynamics are taken from the global circulation module of the ULAQ-CCM (2001–2010), whereas Oslo-CTM3 uses ECMWF forecast meteorology for 2006. The FBC experiments were run for a longer time period (a total of 50 years in both models; 5 consecutive cycles of model years 2001–2010 for the ULAQ model and perpetual year 2006 for Oslo CTM3), allowing the CH_4 mixing ratios to adjust to the OH field, which is in turn perturbed by aircraft NO_x emissions. Background surface fluxes (NO_x, CO, VOCs, FBC-CH_4) and aircraft emissions are kept fixed in the models at values representative of year 2006, as well as surface mixing ratios of long-lived species relevant for the O_3 photochemistry (CFCs, HCFCs, HFCs, N_2O and MBC-CH_4). The FBC experiment used gridded CH_4 fluxes at the surface for natural and anthropogenic sources (IPCC, 2013; Wecht et al., 2014; Lamarque et al., 2010; Bousquet et al., 2011) and the global values are presented in Table 1.

All annual mean values of the aircraft perturbations discussed in this study (*i.e.*, AE-NA or AE*-NA) refer to an average over "steady-state" model years 2001–2010 for the ULAQ model and 2006 for Oslo CTM3. One point that needs to be highlighted is that our study applies to a sustained and constant aviation NO_x emission and for the given background NO_y conditions. The perturbation picture may look different if an increasing trend in aviation NO_x emissions is allowed.

Table 1: CH_4 surface emissions, sinks, global mass burden and lifetime in the models. (a) IPCC (2013); (b) Wecht et al. (2014); (c) Lamarque et al. (2010); (d) Bousquet et al. (2011); (e) same as (d) but scaled up by 16.4 %; (f) EDGAR v4.2 (EC-JRC/PBL, 2011) scaled up by 16.4 %.

Emissions (Tg/yr) Sinks (Tg/yr) Burden (Tg) Lifetime (yr)	**ULAQ-CTM [FBC]**	**Oslo-CTM3 [FBC]**
Natural sources	230[(a–b)]	211[(e)]
[wetlands]	160[(a–b)]	167[(e)]
[termites]	20[(a–b)]-	
[geological]	50[(a)]	44[(e)]
Anthropogenic sources	340[(a–c)]	451[(e–f)]
[agriculture]	125[(a–c)]	174[(f)]
[fossil fuel]	100[(a–c)]	151[(f)]
[waste]	79[(a–c)]	71[(f)]
[biomass burning]	36[(a–c)]	55[(e)]
Total sources	570[(a)]	662[(e–f)]
Soil deposition	30[(a)]	16[(d)]
Atmospheric loss [OH $O(^1D)$ Cl]	540	629
Total sinks	570	645
Global mass burden	4760	4820
Mean lifetime	8.35	7.47

3 Impact on atmospheric chemistry

In this section, we will present the results of the numerical simulations, starting from the short-term aviation impact due to NO_x emissions to the long-term impact due to CH_4 changes, including the troposphere-stratosphere coupling. We will present and discuss the calculated long-term changes of tropospheric and stratospheric O_3 concentrations in the final subsection. The radiative impact will be discussed in Section 4. In addition, we present a systematic model evaluation using available observations or climatological data for key species involved in the chemistry-transport processes relevant for this study, in order to increase the robustness of model findings on the calculated aviation NO_x perturbations.

3.1 NO_x-OH

A summary of the direct aircraft perturbation to tropospheric chemistry is presented in Fig. 1, starting from the average steady-state accumulation of NO_x (= NO + NO_2) (Fig. 1a and 1b) (refer to Søvde et al., 2014 for further details). For the 2006 aircraft emissions, both CTMs calculated a maximum change at the northern mid-latitudes, between approximately 200 and 300 hPa. This change was in the order of 50–100 pptv on an annual basis, with larger values observed in the ULAQ-CTM by approximately a factor of 2, compared

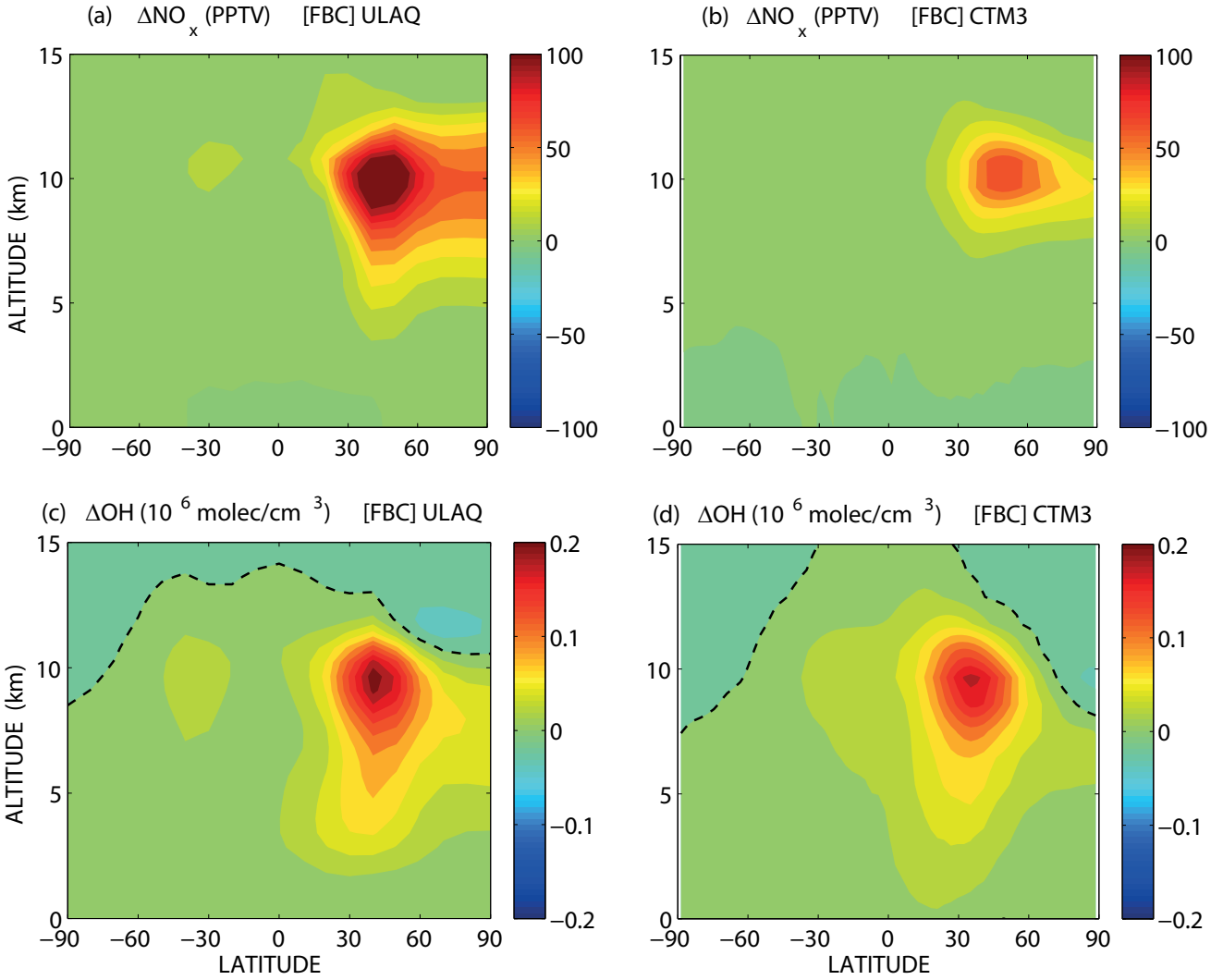

Figure 1: Panels (a, b): Zonal and annual mean of tropospheric NO_x (= NO + NO_2) mixing ratio changes (AE-NA) (pptv), for (a) ULAQ-CTM and (b) Oslo-CTM3. Panels (c, d): as in (a, b), but for tropospheric OH (10^6 molec/cm^3). All panels are for the FBC model experiments.

with Oslo-CTM3. The direct "instantaneous" effect of this NO_x enhancement is to increase the photochemical production of O_3 and OH (Fig. 1c and 1d), the latter largely from the reaction $NO + HO_2 \rightarrow NO_2 + OH$. The models show that the annually averaged maximum increase of OH is 0.15–0.2 $\times$ 10^6 molec/cm^3. A sample evaluation of model results for tropospheric NO_x and NO using data from a collection of aircraft campaigns (Emmons et al., 2000, Schumann et al., 2000) is presented in Fig. 2a and 2b (NO_x) and Fig. 2c and 2d (NO). Solid green and red lines show model profiles at the same latitude and longitude of the campaign, including the variability interval of the observations ($\pm 1\sigma$). The modeled NO_x results have been evaluated at the same time of the year against measurement campaigns PEM-West-A-DC-8 in Japan (Fig. 2a) and POLINAT-2-Falcon in Ireland (Fig. 2b), while the modeled NO against TRACE-P-DC8 in Hawaii (Fig. 2c) and POLINAT-2-Falcon in Canary-Island (Fig. 2d). In general, the modeled vertical profiles conform to the range of variability of measurement data, and this is normally true for all the campaign locations reported in Emmons et al. (2000) and Schumann et al. (2000). Fig. 2 was produced with the ESMValTool (Eyring et al., 2016).

3.2 CH_4-OH

Any attempt to assess the long-term atmospheric response to upper tropospheric NO_x emissions from global aviation requires the calculation of atmospheric CH_4 distribution that allows surface CH_4 to respond freely to tropospheric perturbations of its main sink process, *i.e.*, oxidation by OH. The usual modeling approach of adopting a fixed surface mixing ratio can still be used to calculate aviation-induced changes in CH_4 lifetime, but as previously introduced in Section 1, this does not provide information on the tropospheric mass changes of CH_4 that are caused by upper tropospheric NO_x emissions. In addition, to obtain a meaningful estimate of the lifetime perturbation, the MBC approach necessitates the use of a correction factor, due to the missing feedback of lower tropospheric CH_4 changes on HO_x chemistry (see for example IPCC, 1999; Myhre et al., 2011). The alternative approach of using FBC, would in principle, resolve these issues.

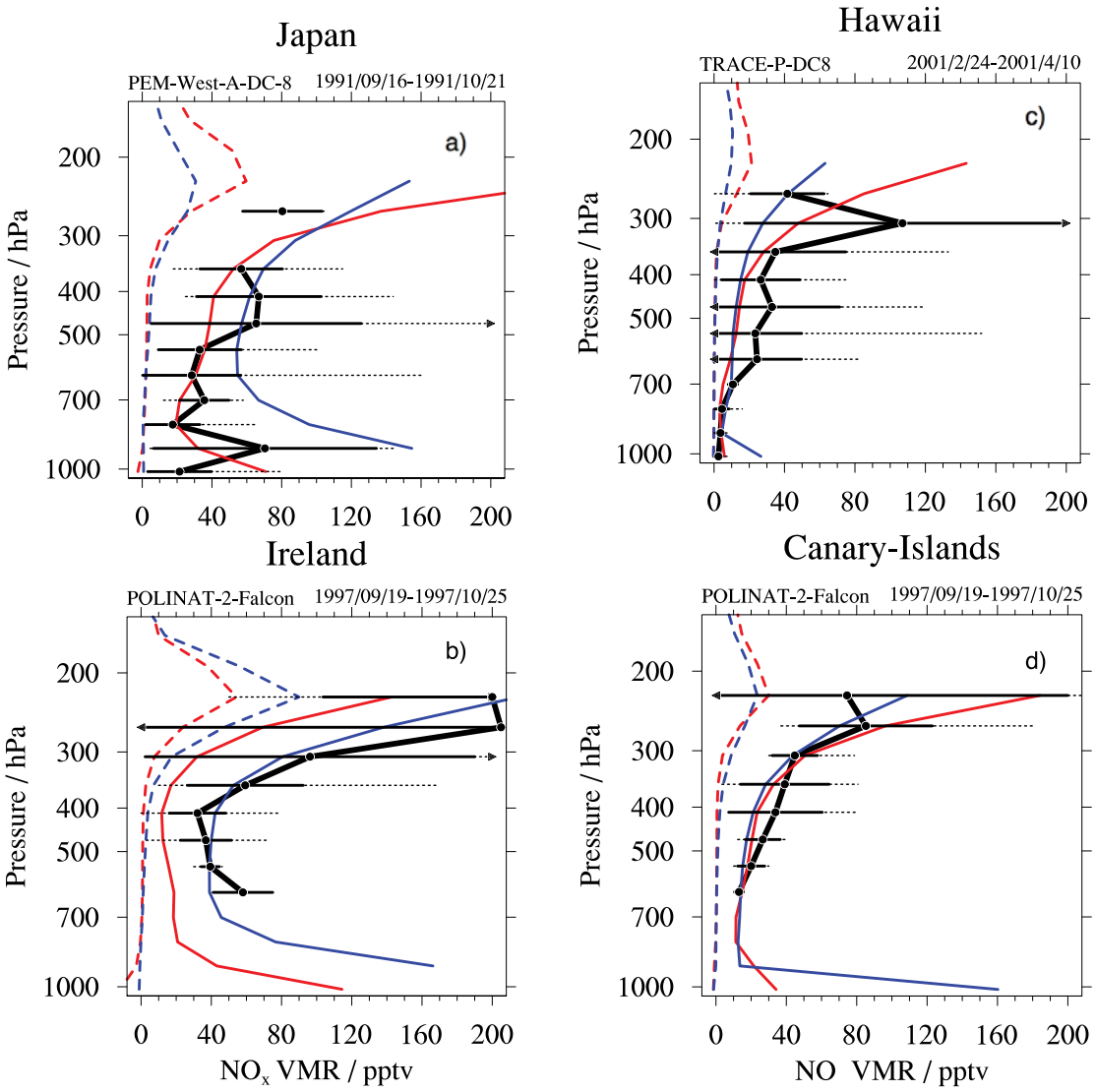

Figure 2: Panels (a, b): tropospheric NO_x evaluation of ULAQ-CTM and Oslo-CTM3 results, using data from a collection of aircraft campaigns (Emmons et al., 2000, Schumann et al., 2000): (a) PEM-West-A-DC8 (Japan, Sept–Oct 1991) and (b) POLINAT-2-Falcon (Ireland, Sept–Oct 1997). Units are in pptv. Panels (c, d): as in (a, b) but for NO mixing ratios, from campaigns (c) TRACE-P-DC8 (Hawaii, Feb–Apr 2001) and (d) POLINAT-2-Falcon (Canary Islands, Sept–Oct 1997). The thick-black solid lines show the observations mean values; the variability intervals are shown with solid whiskers ($\pm 1\sigma$) and dotted whiskers (minimum and maximum). Red and blue solid lines show the FBC AE results of ULAQ-CTM and Oslo-CTM3, respectively. Red and green dashed lines are for the FBC AE-NA changes from the same two models.

3.2.1 Comparison of modeled CH_4 mixing ratio with observations

Annually averaged zonal CH_4 mixing ratios from the FBC experiments (AE case) are presented in Fig. 3a and Fig. 3c, for ULAQ and Oslo models respectively, while the observations from the Aura TES thermal infrared radiances at $\lambda = 8\,\mu m$, corrected using co-retrieved N_2O estimates are shown in Fig. 3b (Worden et al., 2012). The tropopause signature was well captured in the FBC model predictions, with a sudden CH_4 decrease due to downward transport of CH_4-poor stratospheric air in the downwelling branch of the extra-tropical Brewer-Dobson circulation. The inter-hemispheric asymmetry was reasonably represented in both models, whereas the positive vertical gradient of mixing ratios in the tropics and in the Southern Hemisphere was not replicated in model predictions. However, as discussed in Worden et al. (2012), a significant bias was found in the TES-retrieved CH_4 values in the upper troposphere with respect to the lower troposphere. A large part of this bias was adjusted by the TES team applying a correction that is based on co-retrieved N_2O estimates. After correction, a residual of 2.8 % bias was still found in the upper troposphere relative to the lower troposphere.

A quantitative point-by-point spatial evaluation of the ULAQ and CTM3 model results for the FBC case is depicted in Fig. 4, where HALOE data (Grooss and Russel, 2005) were used for the lower stratosphere (Fig. 4a), Aura TES satellite observations for the troposphere (Fig. 4c–4e) and both datasets for the tropical upper troposphere and extra-tropical lowermost strato-

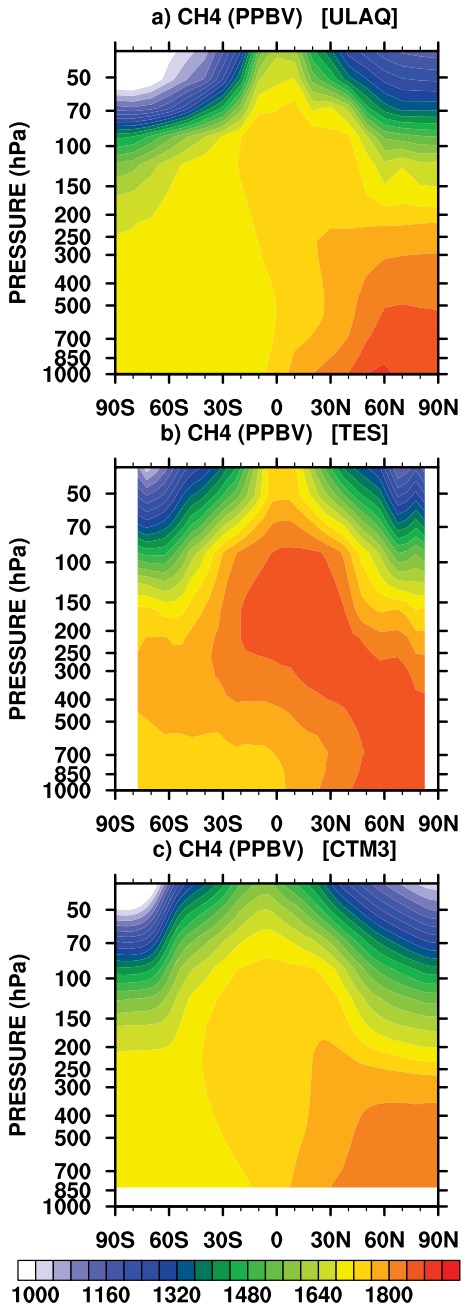

Figure 3: Evaluation of zonal and annual mean CH_4 mixing ratios from the FBC numerical simulations for the AE case of (a) ULAQ-CTM and (c) Oslo-CTM3, using observations from TES Aura radiances (b), averaged over the years 2004–2013 (Worden et al., 2012). Units are in ppbv.

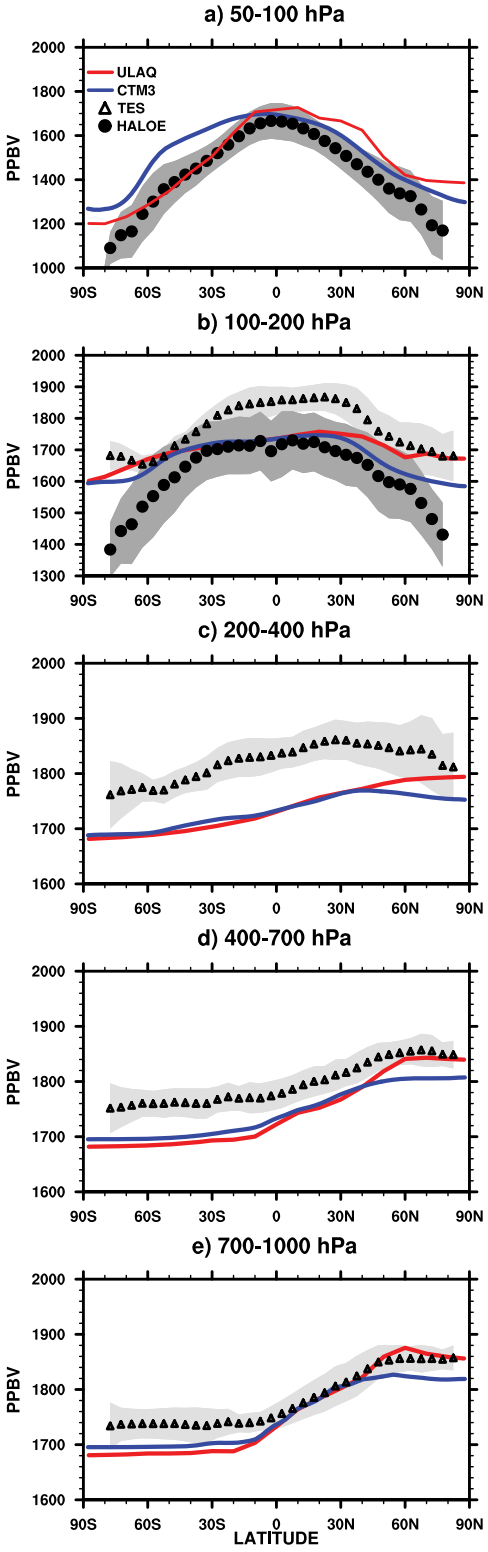

Figure 4: Evaluation of annually averaged latitudinal sections of CH_4 mixing ratios (FBC AE case results) from ULAQ-CTM (red line) and Oslo-CTM3 (blue line), using observations from HALOE in the lower stratosphere (panel a) (Grooss and Russell, 2005), from TES Aura radiances in the troposphere (panels c–e) (Worden et al., 2012) and from both sources in the tropical upper troposphere and extra-tropical lowermost stratosphere (panel b). The shaded areas are $\pm 1\sigma$ of the climatological zonal mean values of HALOE and TES data, averaged over the years 1991–2005 and 2004–2013, respectively.

sphere (Fig. 4b). An average inter-hemispheric difference of 7.5 % was calculated in the mid-troposphere, which was ~ 50 % larger than the observations, where an average of 5 % inter-hemispheric difference was found. Mixing ratios in the Southern Hemisphere were underestimated in the models by approximately 50 to 100 ppbv. This may be attributed to a slower horizontal eddy mixing in the tropical troposphere, with respect to real atmosphere. However, considering also the above discussed residual positive bias of the Aura/TES upper tropospheric CH_4, we may conclude that the inter-

hemispheric gradient in the models is roughly consistent with observations, in their $\pm 1\sigma$ variability interval. By comparing the TES data with HALOE data, the residual bias of TES-retrieved upper tropospheric CH_4 mixing ratio is clearly visible in Fig. 4b. The models are generally within the HALOE data's 1σ uncertainty interval and thus, showing that the models have a good ability in capturing the strong horizontal gradient in the lower stratosphere, pointing out a good isolation of the tropical pipe in the models.

3.2.2 CH_4 lifetime

The major atmospheric sink of CH_4 is the reaction with OH and this determines the CH_4 lifetime, except for an additional smaller contribution from soil deposition (see Table 1) and an additional stratospheric sink due to CH_4 reactions with $O(^1D)$ and Cl. The calculated OH abundance is then critical in the determination of a realistic global burden and lifetime of CH_4. Annual zonal average of OH mixing ratios in the troposphere are presented in Fig. 5a and 5c for the ULAQ and Oslo models respectively, while Fig. 5b shows the climatological values of mean annual values from Spivakovsky et al. (2000). The Oslo-CTM3 tends to overestimate OH in the boundary layer of the Northern Hemisphere subtropics and mid-latitudes, most probably due to an excess of surface NO_x emissions.

The horizontally averaged surface mixing ratio predicted in the ULAQ model for the FBC and MBC experiments is 1754 ppbv, while CTM3 predicted surface mixing ratio is 1774 ppbv for FBC and 1769 ppbv for the MBC experiment (see Table 2). The calculated global lifetime (τ) from the FBC experiment is 8.35 and 7.47 years for the ULAQ and Oslo models respectively. These values are comparable to the value from the SPARC multi-model assessment of atmospheric lifetimes of 8.7 ± 1.4 years (Chipperfield et al., 2013). The expected deviation in global CH_4 mass burden changes due to aviation NO_x emissions is given by $d = \exp(=50/\tau)$, and this was found to be $\sim 0.25\,\%$ and $\sim 0.12\,\%$ for the steady state results of ULAQ and Oslo models respectively.

The CH_4 global burden response to aircraft NO_x emissions of 0.71 Tg-N/yr from the two CTMs used in this study is presented in Fig. 6 as a function of time. The results from a tropospheric 2D CTM, TROPOS-2D (Hough and Johnson, 1991; Skowron et al., 2009), with a global aircraft NO_x emission perturbation of 0.80 Tg-N/yr is also shown in Fig. 6. Here, the larger asymptotic difference in the CH_4 burden from TROPOS-2D in comparison with the ULAQ and Oslo model results, is likely due to a combination of factors; essentially the larger NO_x perturbation applied (0.80 instead of 0.71 Tg-N/yr), and the longer CH_4 lifetime (10.1 instead of 7.9 years). The steady state burden change of −88 Tg is consistent with that in the 3D CTMs ($-88 \times 0.71/0.80 \times 7.9/10.1 = -61$ Tg). Therefore, TROPOS-2D produced an aircraft-induced

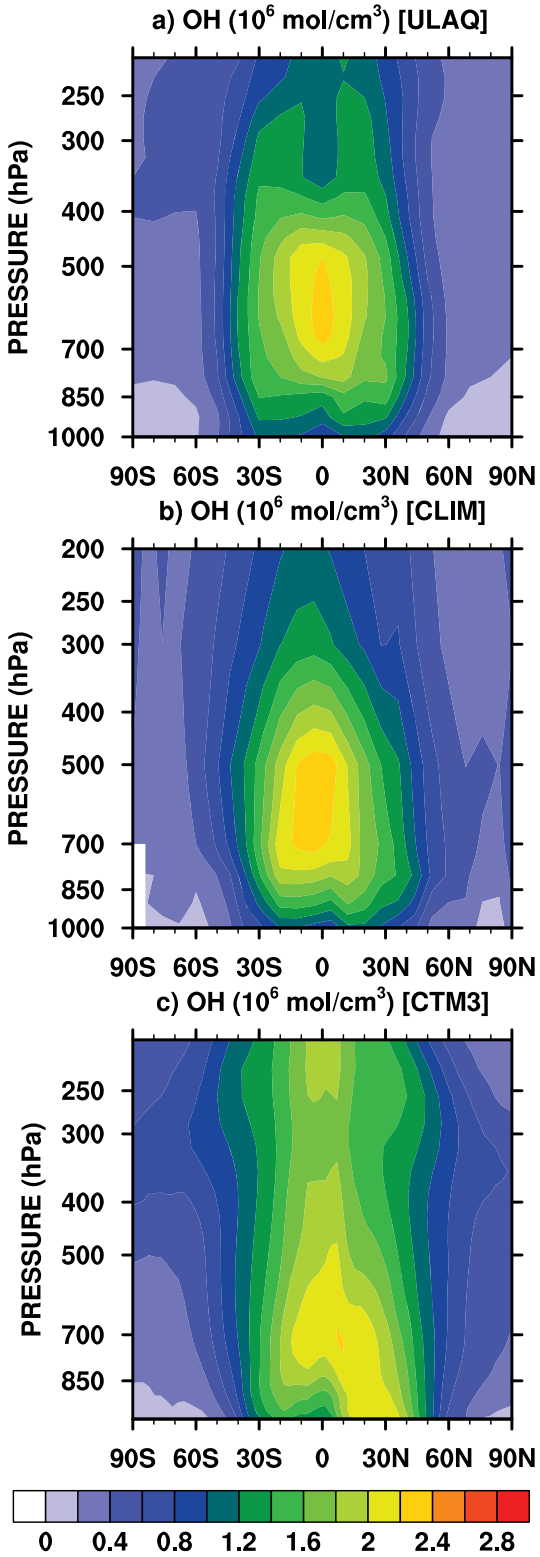

Figure 5: Evaluation of zonal and annual mean OH concentrations (10^6 molec/cm^3) from the FBC numerical simulations (AE case) for (a) ULAQ-CTM and (c) Oslo-CTM3, with a climatology derived in Spivakovsky et al. (2000) (panel b).

CH_4 lifetime change of $-1.8\,\%$ instead of $-1.24 \pm 0.07\,\%$ calculated from the 3D CTMs. Note that the uncertainty expressed here indicates the spread of values between the ULAQ-CTM and Oslo-CTM3 results.

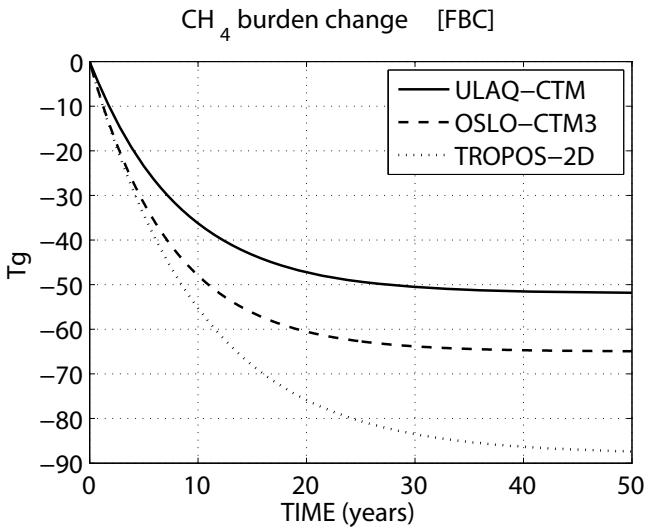

Figure 6: Calculated CH_4 global burden change (AE-NA) as a function of time in response to aircraft NO_x emissions of 0.71 Tg-N/yr in the ULAQ-CTM (solid line) and in the Oslo-CTM3 (dashed line) and in response to aircraft NO_x emissions of 0.80 Tg-N/yr in the TROPOS-2D model (dotted line). The ULAQ-CTM has mean background CH_4 lifetime of 8.35 years and a lifetime change of −1.17 % (AE-NA); the Oslo-CTM3 has mean background CH_4 lifetime of 7.47 years and a lifetime change of −1.32 % (AE-NA); the TROPOS-2D model has a mean background CH_4 lifetime of 10.1 years and a lifetime change of −1.8 % (AE-NA).

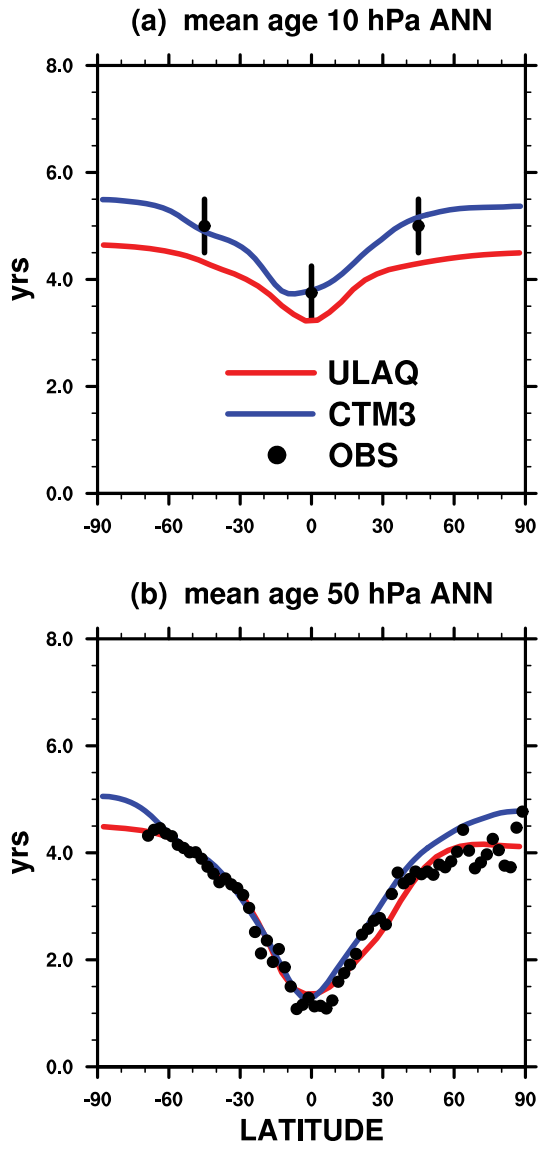

Figure 7: Evaluation of the mean age of air (years), from ULAQ-CTM (red) and Oslo-CTM3 (blue), at (a) 10 hPa and (b) 50 hPa. Observed values are based on ER-2 aircraft measurements of CO_2 (Andrews et al., 2001), balloon CO_2 measurements made in northern mid-latitudes (Waugh and Hall, 2002), and satellite measurements of HF and HCl from HALOE (Anderson et al., 2000). Whiskers show the uncertainty in the measurement-derived mean age of air at 10 hPa.

Holmes et al. (2011) has also calculated a CH_4 lifetime change of -1.70 ± 0.35 % with 1.0 Tg-N/yr aircraft NO_x emissions and if the lifetime changes from the ULAQ and Oslo models are scaled up from 0.71 Tg-N/yr to 1.0 Tg-N/yr, a consistent change of -1.75 ± 0.10 % is obtained. In a model simulation that evaluated the atmospheric chemistry sensitivity to the HNO_3-forming channel of HO_2+NO, Gottschaldt et al. (2013) found an approximate −1.3 % reduction of CH_4 lifetime that is due to ∼ 0.85 Tg-N/yr aircraft NO_x emissions. A scaling of the ULAQ and Oslo models' lifetime changes from 0.71 Tg-N/yr to 0.85 Tg-N/yr would imply a change of -1.48 ± 0.08 %. The CH_4 lifetimes calculations from the FBC experiment of both models show that they are comparable to previous studies referenced above and also those summarized in Table 7 of Lee et al. (2010).

3.3 CH_4-H_2O

Most air enters the stratosphere in the tropics and therefore, it is important to simulate the correct balance between ascent and mixing across the subtropical barriers. Transport in this region is critical in determining the stratospheric composition and information on the tropical ascent, vertical diffusion and the tropical-extratropical mixing can be obtained from the vertical propagation of the annual cycle in water vapor, known as the "tape recorder" signal (Hall et al., 1999), as well as from the mean age of air. The latter is the time elapsed since a stratospheric parcel of air was last in contact with the troposphere, and can be calculated from observations of conserved tracers whose concentrations increase approximately linearly over time.

Observations of CO_2 and SF_6 have been used in previous studies to derive empirical estimates of the mean age of air and to qualitatively evaluate model representations of the residual circulation and mixing (Hall et al., 1999; Eyring et al., 2006). Age of air observations in Fig. 7 are based on ER-2 aircraft measurements of CO_2 (Andrews et al., 2001), balloon CO_2 measurements made in northern mid-latitudes (Waugh and Hall, 2002) and satellite measurements from HALOE (Anderson et al., 2000).

Table 2: Summary of CH_4 model calculations and AE-NA differences (annual-global averages).

Model	Experiment	Surface mixing ratio [ppbv]	Tropospheric mixing ratio [ppbv]	Mass burden [Tg]	Lifetime [years]	Experiment	Tropospheric mixing ratio change [ppbv]	Lifetime change [%]
ULAQ-CTM	FBC	1754	1732	4760	8.35	FBC AE-NA	−18.7	−1.17
ULAQ-CTM	MBC	1754	1735	4765	8.36	MBC AE-NA	−0.27	−0.81
Oslo-CTM3	FBC	1774	1754	4820	7.47	FBC AE-NA	−23.7	−1.32
Oslo-CTM3	MBC	1769	1756	4826	7.67	MBC AE-NA	−0.13	−0.96

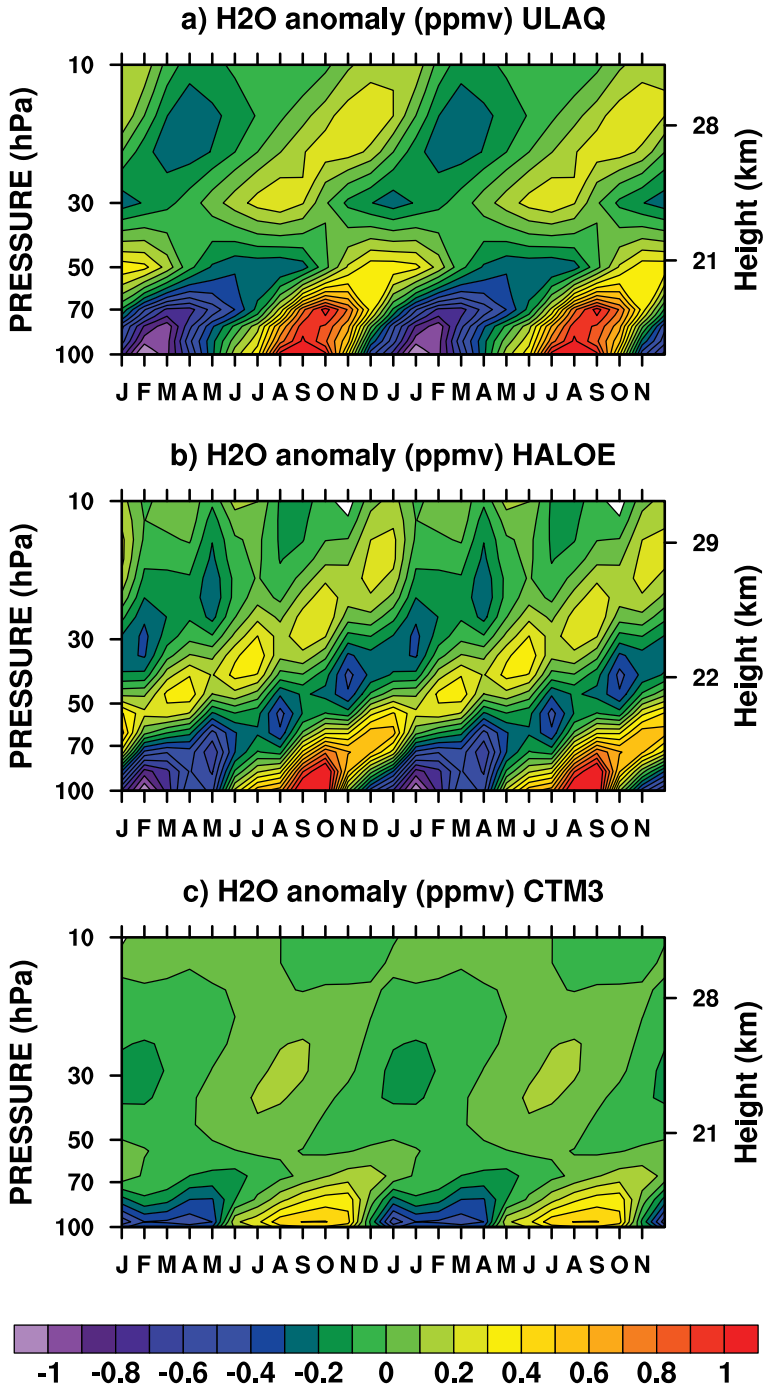

Figure 8: Evaluation of tropical stratospheric H_2O tape recorder signals in ppmv from (a) ULAQ-CTM and (c) Oslo-CTM3 results, using (b) HALOE data. Plotted values are monthly mean tropical anomalies of H_2O (10S-10N) averaged over the years 1991–2005.

These observations are compared with the ULAQ and CTM3 results. Fig. 7 shows that both models compared well with the observations data for mean age of air at 50 hPa at all latitudes (panel b), while the ULAQ model tend to underestimate at 10 hPa (panel a), but still close to the lower limit of the uncertainty interval. The deviation of the water vapor mixing ratio from the monthly mean profile averaged over 10S to 10N for combined HALOE and MLS observations is depicted in Fig. 8b, and for the ULAQ and CTM3 models in Fig. 8a and Fig. 8c respectively. As noted before, the two models represent in a reasonable way the pronounced isolation of the tropical pipe above the tropical tropopause layer (TTL), which is essential to reproduce a realistic tape recorder signal. The Oslo model, however, shows fewer minima, indicating either a faster tropical upwelling or a stronger vertical diffusion and/or a stronger horizontal eddy mixing. The models' reasonable representation of tracer transport in the lower-mid stratosphere can be deduced from both the calculated age of air and the water vapor tape recorder signal. Fig. 8 was produced with the ESMValTool (Eyring et al., 2016).

The instantaneous OH perturbation plays a key role in the global atmospheric chemistry by decreasing the CH_4 lifetime and then linking together short- and long-term effects of aircraft emissions. This is clearly visible in Fig. 9a and 9b, where the CH_4 mixing ratio aircraft perturbation for the FBC experiments is shown. Due to the OH change depicted in Fig. 1c and 1d, a non-negligible inter-hemispheric gradient of the CH_4 perturbation is visible, even though CH_4 is quite well-mixed in the troposphere due to its long lifetime. Conservation of the global hydrogen mass among the main H reservoirs (CH_4, H_2O and H_2), requires the average tropospheric CH_4 change due to aircraft NO_x emissions to be conserved in the stratosphere as the sum of $\Delta CH_4 + 0.5\Delta H_2O + 0.5\Delta H_2$ (Fig. 9c and 9d), thus becoming the driver for photochemical changes of stratospheric water vapor (Fig. 9e and 9f). A more pronounced isolation of the tropical pipe is visible in the ULAQ model with respect to Oslo and this is consistent with what shown in Fig. 8 for the tape recorder signal.

A comparison of FBC and MBC H_x anomalies can be made in Fig. 9c and 9d. In the MBC approach the surface mixing ratio of CH_4 is kept fixed in both AE and NA cases and as a consequence the upper tropospheric OH change forced by the aviation NO_x perturbation cannot produce a mass density adjustment of CH_4 over the whole troposphere, due to its long lifetime. The H_x perturbations (CH_4, H_2O, H_2) are approximately two orders of magnitude smaller in the MBC approach with respect to FBC, due to the zero AE-NA difference at the surface in the MBC approach. This represents the key point in our study, pointing out the importance of letting CH_4 to evolve freely in the whole atmosphere, following the mid-upper tropospheric OH increase induced by the aviation NO_x. The use of a fixed CH_4 surface mixing ratio (*i.e.*, the MBC case) only allows the calculation of CH_4 lifetime perturbation and not the tropospheric CH_4 mass distribution changes (see Table 2). The lifetime change may be underestimated by a factor of 1.41, as an average from the ULAQ and Oslo models, and this can be attributed to the missing feedback of CH_4 changes with the HO_x chemistry (IPCC, 1999).

A comparison of the H_2O model results with satellite data in the stratosphere is presented in Fig. 10. The high-latitude vertical profiles calculated by the models (Fig. 10a and 10b) are in reasonable agreement with HALOE observations. The Antarctic springtime dehydration is well represented in the ULAQ-CTM, with mixing ratio values down to 2 ppmv at 70–100 hPa in October, compared with 4 ppmv in the same layer over the Arctic in March. It can be seen in the latitudinal sections of Fig. 10c that the Oslo-CTM3 water vapor distribution in the mid-lower stratosphere compared well with HALOE observations, whereas the ULAQ-CTM H_2O values are low-biased by ~ 5–15 %. However, both models correctly capture the amplitude of the pole to equator horizontal gradient, which is an indication of a realistic coupling of horizontal mixing and tropical upwelling (Strahan et al., 2011).

3.4 NO_x-HO_x-O_3

The stratospheric decrease of water vapor described in Section 3.2, produces a negative anomaly of HO_x (directly) and a positive anomaly of NO_x (indirectly) that is caused by the reaction $NO_2 + OH + m \rightarrow HNO_3 + m$ and thus, acting as the most important NO_x sink in the stratosphere. Fig. 11a–f present the effects of the water vapor anomaly on HO_x and NO_x stratospheric changes as FBC-MBC, since no significant tropospheric CH_4 mixing ratio changes can be calculated in the MBC (AE-NA) experiment. Inter-model differences in the anomalies of stratospheric OH (Fig. 11a and 11b) and tropospheric HO_2 (Fig. 11c and 11d) can be explained in term of inter-model differences in the distribution of the NO_x anomalies. The latter are often attributed to the difference in the models' ability to export tropospheric NO_x into the stratosphere above the TTL. Fig. 9 shows that the stratospheric H_2O perturbation is a result of tropospheric CH_4 mixing ratio adjustment to direct aircraft emission of NO_x. Therefore, the stratospheric FBC-MBC of HO_x and NO_x for the AE-NA perturbations represents the driver of long-term O_3 responses to aircraft emissions, both in the troposphere and stratosphere.

The NO_x enhancement in Fig. 11e and 11f drives an O_3 decrease in the mid-stratosphere, where it acts as an O_3 depleting species in the classical NO_x catalytic cycle (Fig. 12a). On the other hand, the HO_2 lower stratospheric decrease of Fig. 11c and 11d has the net effect of lowering the O_3 production term $k[NO][HO_2]$ (Fig. 12b). Both these effects lead to a reduction of stratospheric O_3 (Fig. 13). However, this is only visible in the FBC case and absent or much smaller in the MBC case, since the tropospheric CH_4 decrease is significant in the long-term and thus, triggering the long-term

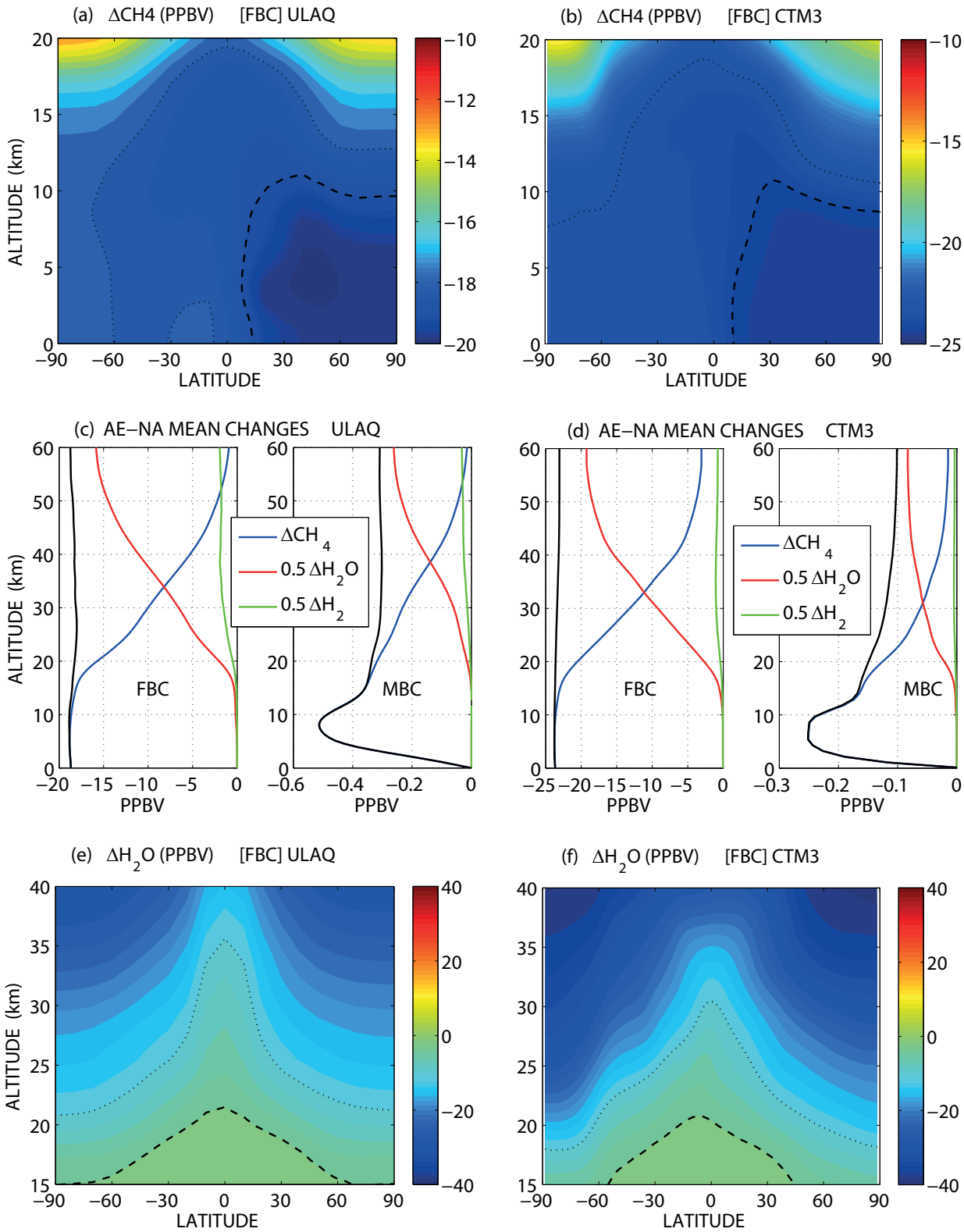

Figure 9: Panels (a, b): Zonal and annual mean of tropospheric CH_4 mixing ratio changes (AE-NA) (ppbv), for (a) ULAQ-CTM and (b) Oslo-CTM3. Dashed and dotted lines highlight contour lines of −19 and −18 ppbv respectively in Panel (a), and 24 and 23 ppbv respectively in Panel (b). Color scales and highlighted contour line are different because the CH_4 change due to aviation emission of NO_x is slightly different in the two models (see Table 2 and Fig. 5). Panels (c, d): Horizontally averaged AE-NA mean annual changes of CH_4 (blue line), $0.5H_2O$ (red line), $0.5H_2$ (green line) and total net (black line), for (c) ULAQ-CTM and (d) Oslo-CTM3, with results of the FBC case on the left hand side of panels (c,d) and results of the MBC case on the right hand side. Panels (e, f): Zonal and annual mean of stratospheric H_2O mixing ratio changes (AE-NA) (ppbv), for (e) ULAQ-CTM and (f) Oslo-CTM3. Dashed and dotted lines highlight contour lines of −2 and −10 ppbv respectively. All panels are for the FBC model experiments.

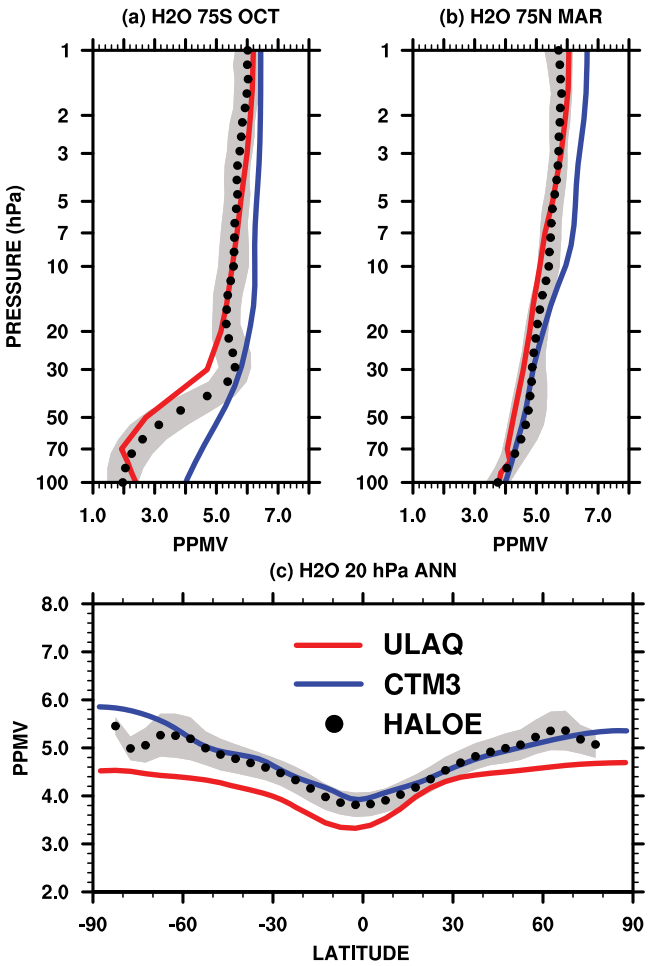

Figure 10: Stratospheric H_2O evaluation of ULAQ-CTM (red) and Oslo-CTM3 (blue) results, using HALOE data (dots) (Grooss and Russell, 2005). Panels (a, b) show springtime polar vertical profiles from 1 to 100 hPa at 75S (October) and 75N (March) respectively. Panel (c) shows a latitudinal section at 20 hPa as an annual average. The grey areas show $\pm 1\sigma$ of the climatological zonal mean values (averaged over the years 1991–2005)

stratospheric effects on H_2O and O_3. In the MBC case, small positive/negative O_3 changes in the lower/mid stratosphere (respectively) are short-term effects due to a limited penetration of tropospheric aircraft NO_x in the lower stratospheric tropical pipe (Rogers et al., 2002). This effect may slightly increase the short-term O_3 production/loss at altitudes that are below/above (respectively) the so-called turnover point of O_3 production from NO_x anomalies (Pitari et al., 2008).

The negative O_3 changes in AE-NA, obtained from FBC-MBC, represent the long-term O_3 response to the changing atmospheric HO_x distribution produced by the CH_4 adjustment to the OH field perturbed by aircraft NO_x emissions. Upper tropospheric O_3 anomalies of the order of −0.5 ppbv are calculated in both model simulations (Fig. 14a and 14b). The corresponding long-term stratospheric O_3 anomalies AE-NA (from FBC-MBC) are presented in Fig. 14c and 14d and these are consistent with the AE-NA FBC-MBC anomalies of HO_x and NO_x in Fig. 11. The maximum long-term decrease of O_3 production in the extra-tropics is found below the altitude of 20 km, while a maximum long-term increase of O_3 destruction in the tropics is found above 30 km. These stratospheric anomalies will produce a long-term negative correction to the aviation O_3 radiative forcing, normally referred to as PMO-RF, *i.e.*, primary mode O_3 radiative forcing, with the largest values in the extra-tropics (to be discussed in detail in the following section).

An evaluation of the model calculated O_3 fields has been made using HALOE and TES/Aura satellite data, as shown in Fig. 15. Springtime high-latitude vertical profiles indicate that both models are successful in capturing the lower stratospheric O_3 depletion forced by the large concentrations of halogen species (Fig. 15a and 15b) (Austin et al., 2010). The large latitudinal gradients of the O_3 mixing ratio are also well captured by the models in the lower stratosphere (Fig. 15c), upper stratosphere and lowermost stratosphere (Fig. 15d) and finally in the mid-upper troposphere (Fig. 15e). It is worth noting that the O_3 retrieval from TES/Aura radiances in the upper troposphere and lowermost stratosphere features the same tendency to overestimate the chemical tracer with respect to HALOE observations, as illustrated by the TES/Aura CH_4 in Fig. 4b.

4 Radiative forcing

The ULAQ-CCM radiative transfer module (ULAQ-RTM) was applied offline to the monthly averaged fields of O_3, CH_4 and stratospheric H_2O calculated by the ULAQ and Oslo models and the RF results are presented in Table 3a and 3b respectively. NO_2 and aerosol data were also used in the ULAQ-RTM, the latter only from the ULAQ-CTM calculations.

4.1 Short-term O_3 and PMO

The O_3 RF breakdown between tropospheric and stratospheric contributions makes it possible to calculate the long-term effects for the two regions by comparing the results of MBC and FBC model experiments. In the MBC case, where CH_4 is fixed at the surface, the lifetime change is due to the NO_x-driven OH enhancement and therefore, it is not able to trigger a realistic CH_4 decrease and consequently, a related loss of stratospheric H_2O. Thus, the O_3 RF is a pure "instantaneous" response to aviation NO_x, *i.e.*, short-term O_3. This is 15.17 mW/m^2 and 19.41 mW/m^2 for the ULAQ-CTM and Oslo-CTM3 models respectively. These short-term O_3 RFs are smaller than those reported in Søvde et al. (2014) and Pitari et al. (2015) due to an updated and more realistic setup of tropospheric cloudiness in the ULAQ-RTM.

The difference between MBC and FBC gives an indirect estimate of the long-term impacts of aviation

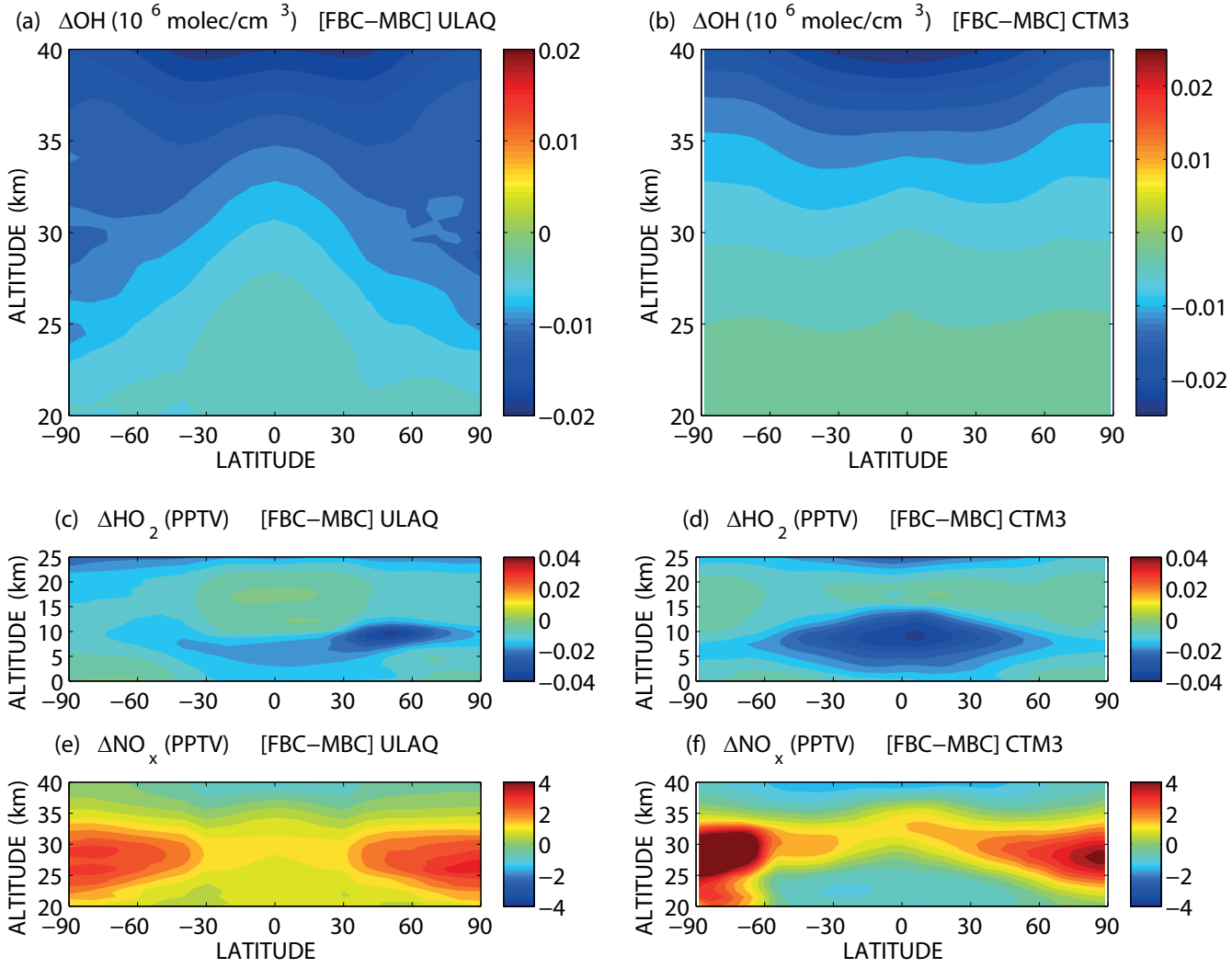

Figure 11: Panels (a, b): Zonal and annual mean of long-term stratospheric OH concentration changes (AE-NA, FBC-MBC) (10^6 molec/cm^3), for (a) ULAQ-CTM and (b) Oslo-CTM3. Panels (c, d): Zonal and annual mean of long-term tropospheric and lower stratospheric HO_2 mixing ratio changes (AE-NA, FBC-MBC) (pptv). Panels (e, f): Zonal and annual mean of long-term stratospheric NO_x (= NO + NO_2) mixing ratio changes (AE-NA, FBC-MBC) (pptv). All panels show FBC-MBC values that represent the long-term atmospheric response to aircraft emissions of NO_x, via CH_4 adjustment to the tropospheric OH perturbation.

NO_x on both tropospheric and stratospheric O_3 (see Table 3a and 3b). The long-term tropospheric O_3 RF calculated by the ULAQ-RTM is $-3.91\,mW/m^2$ for the ULAQ-CTM results and $-3.94\,mW/m^2$ for the Oslo-CTM3. This represented 47 % (ULAQ-CTM) and 38 % (Oslo-CTM3) of the CH_4 RF calculated by the ULAQ-RTM, and 52 % (ULAQ-CTM) and 46 % (Oslo-CTM3) of the CH_4 RF calculated with the Myhre et al. (2011) parametric lifetime formula. The parametric formula of Myhre et al. (2011) expresses the CH_4 RF as a function of the percentage lifetime change: $CH_4\text{-RF}(mW/m^2) = \chi\text{-}CH_4(ppbv) \times 0.37 \times \Delta\tau\text{-}CH_4(\%)/100$, where $\Delta\tau$ is the lifetime change (AE-NA) and χ is the tropospheric mixing ratio. It was used to estimate the CH_4 RF in the MBC case. An average feedback factor of 1.4 was applied to the tropospheric CH_4 mixing ratio to account for the CH_4 adjustment to the upper tropospheric OH perturbation, since the model prediction was made using a fixed mixing ratio boundary condition at the surface. Table 4 also shows that the ratio of the long-term tropospheric O_3 RF to that of CH_4 RF are within the 50 ± 27 % estimated by Myhre et al. (2013) for primary mode ozone (PMO). This is the long-term response of tropospheric O_3 to the change in CH_4 distribution and its impact on HO_x chemistry, and on tropospheric O_3 production from NO + HO_2 and NO + CH_3O_2 (Wild et al., 2001).

4.2 CH_4 and long-term stratospheric H_2O and O_3

The CH_4 RF computed through a radiative transfer code could be higher by 10–20 % than those calculated using parameterizations that are based on the average tropospheric mixing ratio and lifetime change (Myhre et al., 1998). This trend was also observed in the FBC case (Tables 3a and 3b), where for the ULAQ model, the RF decreased from $-8.38\,mW/m^2$ (from RTM) to $-7.50\,mW/m^2$ (from parameterization) and for the Oslo

Table 3a: Summary of ULAQ-CTM NO_x-related RF terms (global averages): O_3, CH_4, stratospheric H_2O, NO_2, NO_3^-,$SO_4^=$ and net from NO_x emissions (*i.e.*, AE-NA). The six columns show, respectively: species, type of experiment, species global changes, shortwave RF, adjusted longwave RF, net RF. All RFs are calculated at the tropopause in total sky conditions with stratospheric temperature adjustment and with the ULAQ radiative transfer module (see text for details). The short-term O_3 perturbation is obtained from the MBC model run; trop-strat long-term O_3 perturbations are obtained as difference between FBC and MBC model runs. Global changes of gas species are shown in terms of delta-column in Dobson Units (DU), except for CH_4: here the average tropospheric mixing ratio change is reported (ppbv), along with the lifetime perturbation (%). Global changes of the aerosol components (NO_3^-, $SO_4^=$ and SOA) are shown in terms of the optical depth (AOD) at $\lambda = 0.55\,\mu$m. The indirect forcing of aerosols on warm clouds is parameterized using scaling factors with respect to direct forcing, as recommended in Fuglestvedt et al. (2008). For nitrate, the mass fraction coated on soil dust is not considered in the indirect forcing, due to the low dust hygroscopicity (Bauer et al., 2007).

Species	EXP	Global changes [DU] for gases AOD for aerosols	RF-SW [mW/m^2]	RF-LWadj [mW/m^2]	RF-NET [mW/m^2]
O_3 total	FBC	0.26	3.79	6.37	10.16
	MBC	0.46	4.02	11.15	15.17
O_3 troposphere	FBC	0.32	3.23	6.80	10.03
	MBC	0.43	4.16	9.78	13.94
O_3 stratosphere	FBC	−0.06	0.56	−0.43	0.13
	MBC	0.03	−0.14	1.37	1.23
O_3 short-term	MBC	0.46	4.02	11.15	15.17
O_3 long-term trop	FBC-MBC	−0.11	−0.93	−2.98	−3.91
O_3 long-term strat	FBC-MBC	−0.09	0.70	−1.80	−1.10
CH_4	FBC	−18.7 ppbv [trop]	0.0	−8.38	−8.38
		−1.17 % [lifetime]	0.0	−7.50	−7.50 [lifetime]
	MBC	−0.27 ppbv [trop]	–	–	–
		−0.81 % [lifetime]	0.0	−7.50	−7.50 [lifetime]
CO_2 from CH_4 oxidation [50 year time horizon]	FBC	−1.9 ppbv/yr	–	−1.34	−1.34
	MBC	−0.03 ppbv/yr	–	−0.02	−0.02
H_2O stratosphere	FBC	−0.57	0.15	−1.49	−1.34
	MBC	−0.01	0.00	−0.01	−0.01
NO_2	FBC	3.7×10^{-4}	0.28	0.43	0.71
	MBC	3.6×10^{-4}	0.27	0.41	0.68
NO_3^-	FBC	6.2×10^{-5}	−1.98	0.26	−1.72
	MBC	5.2×10^{-5}	−1.60	0.25	−1.35
$SO_4^=$aerosols from increase of oxidants (OH, H_2O_2, O_3)	FBC	2.5×10^{-4}	−4.29	1.22	−3.07
	MBC	2.6×10^{-4}	−4.49	1.31	−3.18
SOA from increase of oxidants (NO_3, OH, O_3)	FBC	1.0×10^{-5}	−0.22	0.02	−0.20
	MBC	0.8×10^{-5}	−0.18	0.01	−0.17
Aerosol indirect effect on warm clouds	FBC		−1.07	–	−1.07
	MBC		−0.96	–	−0.96
NET from NO_x	FBC		−3.34	−2.91	**−6.25**
	MBC		−2.94	5.60	2.66

model from −10.35 mW/m^2 (RTM) to −8.57 mW/m^2 (parameterization). The difference is mainly due to the inclusion of solar near-infrared contribution in the 4–10 µm wavelength band, and partly due to the inhomogeneity of the CH_4 spatial distribution. In the FBC case, it was not necessary to include the 1.4 feedback factor to the tropospheric CH_4 mixing ratio since the CH_4 RF was calculated from the mixing ratio change itself. In Tables 3 we also show the RF contribution of CO_2 from the products of CH_4 oxidation, on a 50 year time horizon, by calculating the difference in CO_2 accumulation (in ppbv/yr) for ULAQ and Oslo models.

The changing tropospheric CH_4 distribution has a direct feedback on stratospheric water vapor, because

Table 3b: As in Table 3a, but for Oslo-CTM3 calculations, using the ULAQ-RTM for RFs. The direct and indirect contributions of NO_3^-, $SO_4^=$ and SOA are calculated in ULAQ-CTM (see Table 3a).

Species	EXP	Global changes [DU]	RF-SW [mW/m^2]	RF-LWadj [mW/m^2]	RF-NET [mW/m^2]
O_3 total	FBC	0.36	4.41	9.72	14.13
	MBC	0.61	4.25	15.16	19.41
O_3 troposphere	FBC	0.45	3.69	10.67	14.36
	MBC	0.56	4.66	13.63	18.29
O_3 stratosphere	FBC	−0.09	0.72	−0.95	−0.23
	MBC	0.05	−0.41	1.53	1.12
O_3 short-term	MBC	0.61	4.25	15.16	19.41
O_3 long-term trop	FBC-MBC	−0.11	−0.97	−2.97	−3.94
O_3 long-term strat	FBC-MBC	−0.14	1.13	−2.47	−1.34
CH_4	FBC	−23.7 ppbv [trop]	0.0	−10.35	−10.35
		−1.32 % [lifetime]	0.0	−8.57	−8.57 [lifetime]
	MBC	−0.13 ppbv [trop]	–	–	–
		−0.96 % [lifetime]	0.0	−8.57	−8.57 [lifetime]
CO_2 from CH_4 oxidation [50 year time horizon]	FBC	−2.6 ppbv/yr	–	−1.86	−1.86
	MBC	−0.02 ppbv/yr	–	−0.01	−0.01
H_2O stratosphere	FBC	−0.71	0.17	−1.62	−1.45
	MBC	0.01	0.00	−0.02	−0.02
NO_2	FBC	4.1×10^{-4}	0.30	0.13	0.43
	MBC	4.1×10^{-4}	0.29	0.14	0.43
Net aerosol [ULAQ model]	FBC		−7.57	1.50	−6.07
	MBC		−7.23	1.57	−5.66
NET from NO_x	FBC		−2.69	−2.48	**-5.17**
	MBC		−2.69	8.27	5.58

Table 4: Summary of NO_x-related long-term RF components relative to CH_4 (including also the CO_2 contribution from CH_4 oxidation on a 50 year time horizon), from ULAQ-CTM and Oslo-CTM3 and comparison with IPCC estimates.

Species	Model	Global changes H_2O, O_3 [DU] CH_4 [Tg] CO_2 [ppbv/yr]	RF-NET [mW/m^2]	RF/RF-CH_4 [%]	RF/RF-CH_4 [%] (IPCC, 2013)
CH_4	ULAQ	−52	−8.38	–	–
	CTM3	−66	−10.35	–	–
CO_2 from CH_4 oxidation [50 year time horizon]	ULAQ	−1.9	−1.34	13.8	–
	CTM3	−2.6	−1.86	15.2	–
H_2O stratosphere	ULAQ	−0.57	−1.34	13.8	15 ± 10
	CTM3	−0.71	−1.45	11.9	
O_3 troposphere	ULAQ	−0.11	−3.91	40.0	50 ± 27
	CTM3	−0.11	−3.94	32.3	
O_3 stratosphere	ULAQ	−0.08	−1.10	11.3	–
	CTM3	−0.14	−1.34	11.0	–
O_3 total	ULAQ	−0.20	−5.01	51.5	50 ± 27
	CTM3	−0.27	−5.27	43.2	

Table 5: Summary of RF contributions from aviation NO_x emissions (first two columns) as an average of ULAQ and Oslo model results. Contributions from direct and indirect effects of aerosols are calculated only in the ULAQ model. The last two columns summarize the indirect effects of SO_4 aircraft emissions on NO_x chemistry, via heterogeneous chemistry on $SO_4^=$ aerosol SAD. The uncertainty interval indicates the spread of values between the two models.

Species [NO_x emission]	RF [mW/m^2]	Species [indirect effect of $SO_4^=$ emissions on NO_x chemistry, via heterogeneous chemistry on aerosol SAD]	RF [mW/m^2]
O_3 short-term total	+17.3 ± 2.1	**O_3 short-term total**	−0.80 ± 0.05
O_3 long-term troposphere	−3.92 ± 0.01	**O_3 long-term troposphere**	+0.40 ± 0.05
O_3 long-term stratosphere	−1.2 ± 0.1	**O_3 long-term stratosphere**	+0.05 ± 0.01
CH_4 long-term	−9.4 ± 1.0	**CH_4 long-term**	+0.5 ± 0.1
CO_2 from CH_4 oxidation [50 year time horizon]	−1.6 ± 0.3	**CO_2 from CH_4 oxidation [50 year time horizon]**	+0.10 ± 0.01
H_2O long-term stratosphere	−1.4 ± 0.1	**H_2O long-term stratosphere**	+0.08 ± 0.02
NO_2 total	+0.6 ± 0.1	**NO_2 total**	−0.05 ± 0.01
NO_3^- aerosols	−1.7	**NO_3^- aerosols from increase of HNO_3 [direct + indirect]**	−1.0
$SO_4^=$ aerosols and SOA from increase of oxidants (OH, H_2O_2, O_3, NO_3)	−3.3	**$SO_4^=$ aerosols and SOA from decrease of oxidants (OH, H_2O_2, O_3, NO_3) [direct + indirect]**	+0.2
Indirect effect of aerosols on warm clouds	−1.1	**NET from the indirect effect of $SO_4^=$ emissions on NO_x chemistry**	−0.5 ± 0.1
NET from NO_x emission	−5.7 ± 0.6	**NET from NO_xemissions and the indirect effect of $SO_4^=$ emissions on NO_x chemistry**	−6.2 ± 0.7

of the global amount of hydrogen mass that has to be conserved among the three major reservoir species (mainly CH_4 and H_2O) (Section 3, Fig. 9). The calculated net stratospheric H_2O RFs from the models are −1.34 mW/m^2 and −1.45 mW/m^2 for the ULAQ and Oslo models respectively. They represent the long-term stratospheric response to aircraft NO_x emissions (via OH and CH_4) and are 14 % (ULAQ) and 12 % (Oslo) of the respective CH_4 RF (see Table 4), which are in good agreement with the 15 ± 10 % estimated in Myhre et al. (2007) and Myhre et al. (2013). The use of a fixed mixing ratio boundary condition at the surface almost does not allow changes in photochemical lifetime to feedback on the tropospheric CH_4 mass distribution. The reduction of CH_4 mixing ratios is limited to the upper troposphere and the average decrease below the tropopause was found to be only 0.27 ppbv and 0.13 ppbv for the ULAQ and Oslo models respectively (Table 2). These are only 1.4 % (ULAQ) and 0.5 % (Oslo) of the tropospheric mixing ratio decrease in the FBC case. Therefore, the MBC CH_4 lifetime change (−0.81 % and −0.96 % for the ULAQ and Oslo models respectively) is underestimated when compared with the FBC case (−1.17 % and −1.32 %). The FBC/MBC lifetime change ratio of 1.44 (ULAQ) and 1.38 (Oslo), which are consistent with the factor 1.4 estimated in IPCC (1999), were applied to the aviation CH_4 RF calculated from lifetime perturbation.

As previously discussed in Section 3, the O_3 photochemistry is affected by the decreasing amount of stratospheric H_2O and this effect can only be captured in the FBC experiment (refer to Fig. 11– 12). From Tables 3, we can see that the stratospheric O_3 column change decreases from 0.04 DU in MBC to −0.07 DU in FBC, resulting in the net RF change from +1.17 mW/m^2 to −0.05 mW/m^2 (as an average of the values calculated in ULAQ-CTM and Oslo-CTM3). The stratospheric O_3 RF difference of −1.2 mW/m^2 between the FBC and MBC cases can be defined as the stratospheric O_3 long-term response to aircraft NO_x emissions (via tropospheric OH–CH_4 and then, stratospheric H_2O–HO_x–NO_x). It represents 11 % of the CH_4 RF (see Table 4). The combined tropospheric and stratospheric long-term O_3 effects resulted in a total of approximately 51 % and 43 % of the CH_4 RF from the ULAQ and Oslo models respectively.

As shown in Table 5, the calculated model-average net contribution to RF from aircraft NO_x emissions (−5.7 mW/m^2) is obtained by summing up the instantaneous short-term O_3 RF (+17.3 mW/m^2) (MBC) with the five long-term responses: CH_4 (−9.4 mW/m^2) (FBC), CO_2 from CH_4 oxidation (−1.6 mW/m^2 on a 50 year time horizon) (FBC), tropospheric O_3 (−3.9 mW/m^2) (FBC-MBC), stratospheric H_2O (−1.4 mW/m^2) (FBC), stratospheric O_3 (−1.2 mW/m^2) (FBC-MBC). Alternatively, the net aircraft NO_x RF can be obtained by subtracting the long-term CH_4 (−9.4 mW/m^2), CO_2 from CH_4 oxidation (−1.6 mW/m^2) and stratospheric H_2O (−1.4 mW/m^2) re-

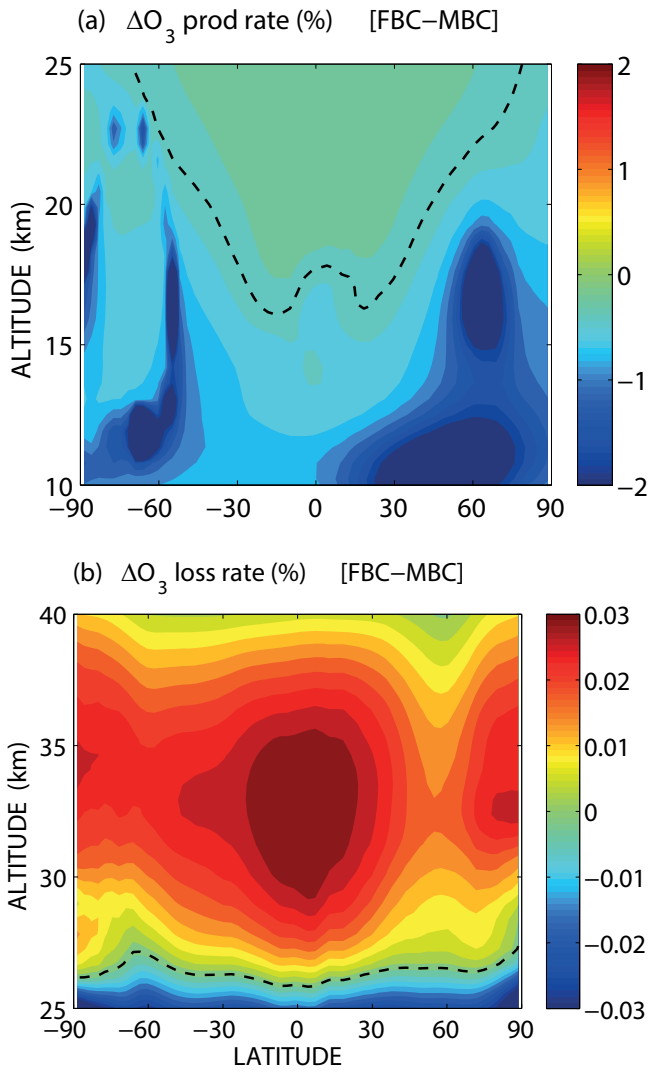

Figure 12: Zonal and annual mean changes (AE-NA) of long-term O_3 (a) production and (b) loss frequency rates, as FBC-MBC percentage of the baseline rates (NA, MBC). The results are shown as an average of ULAQ-CTM and Oslo-CTM3. The dashed line highlights the contour line of −0.3 % in panel (a) and the zero contour line in panel (b).

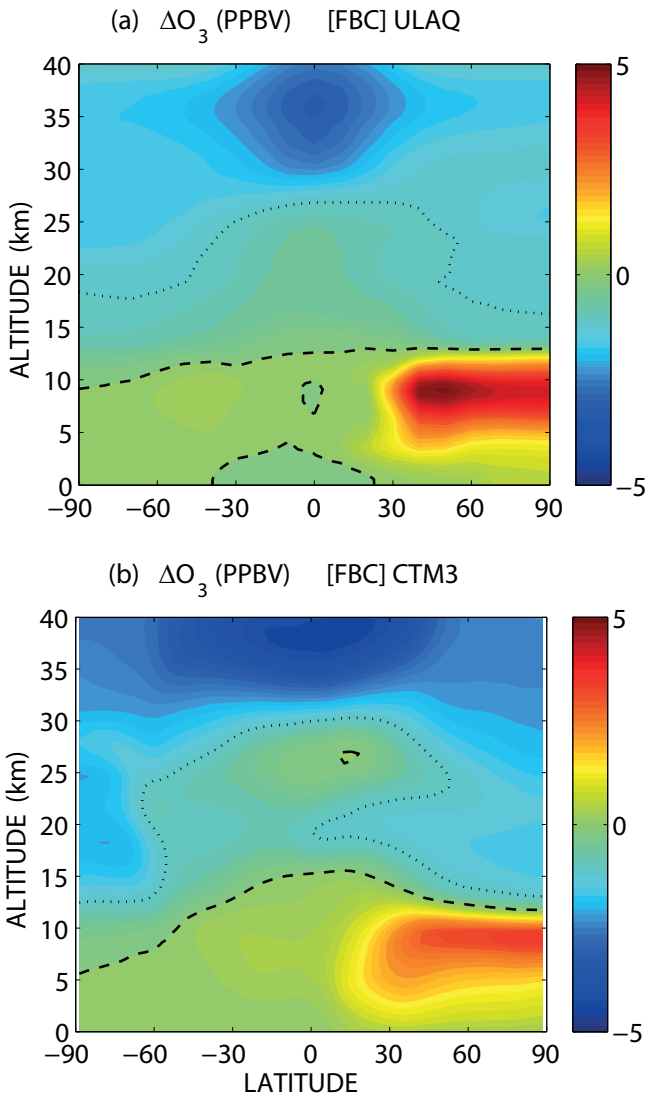

Figure 13: Zonal and annual mean changes (AE-NA, FBC) of O_3 mixing ratio (ppbv) for (a) ULAQ-CTM and (b) Oslo-CTM3. Dashed and dotted lines highlight contour lines of 0 and −1 ppbv respectively.

sponses from the FBC net O_3 RF (+12.2 mW/m^2, short- and long-term). The net gaseous RF from aviation NO_x emissions is obtained by summing up these terms with the short-term contributions from NO_2 (+0.6 mW/m^2), resulting in +0.4 mW/m^2. Finally, the net RF from aviation NO_x emissions is obtained by summing up the ULAQ model calculated aerosol direct and indirect effects (−6.1 mW/m^2) to the net gaseous RF, resulting in −5.7 mW/m^2.

4.3 Aerosols

The impact of NO_x emissions on secondary aerosols (sulfates, nitrates and organics) was calculated only in the ULAQ-CTM, with offline RFs in the ULAQ-RTM. The RF results for these aerosol components are presented in Table 3a and do not include the contribution of direct aerosol emissions by the aircraft (*i.e.*, black carbon and SO_2/SO_4). The impact is produced by the tropospheric enhancement of oxidants (OH, H_2O_2, O_3), resulting in a more efficient SO_2 oxidation in SO_4, and also by increasing the nitrate formation from NO_3 + BVOC (biogenic organics) and HNO_3 heterogeneous reactions on the surface of soil dust or sea salt particles (Ayres et al., 2015).

The indirect forcing of aerosols on warm clouds was not calculated explicitly, but scaled to direct forcing (as recommended in Fuglestvedt et al., 2008 from the results of Kvalevåg and Myhre, 2007). This is the only physical process not explicitly resolved in our study, but parameterized with scaling factors: on the other hand, a proper detailed treatment of aerosol-cloud interactions is beyond the purposes of the present study. For nitrates, the mass fraction coated on soil dust is not considered in

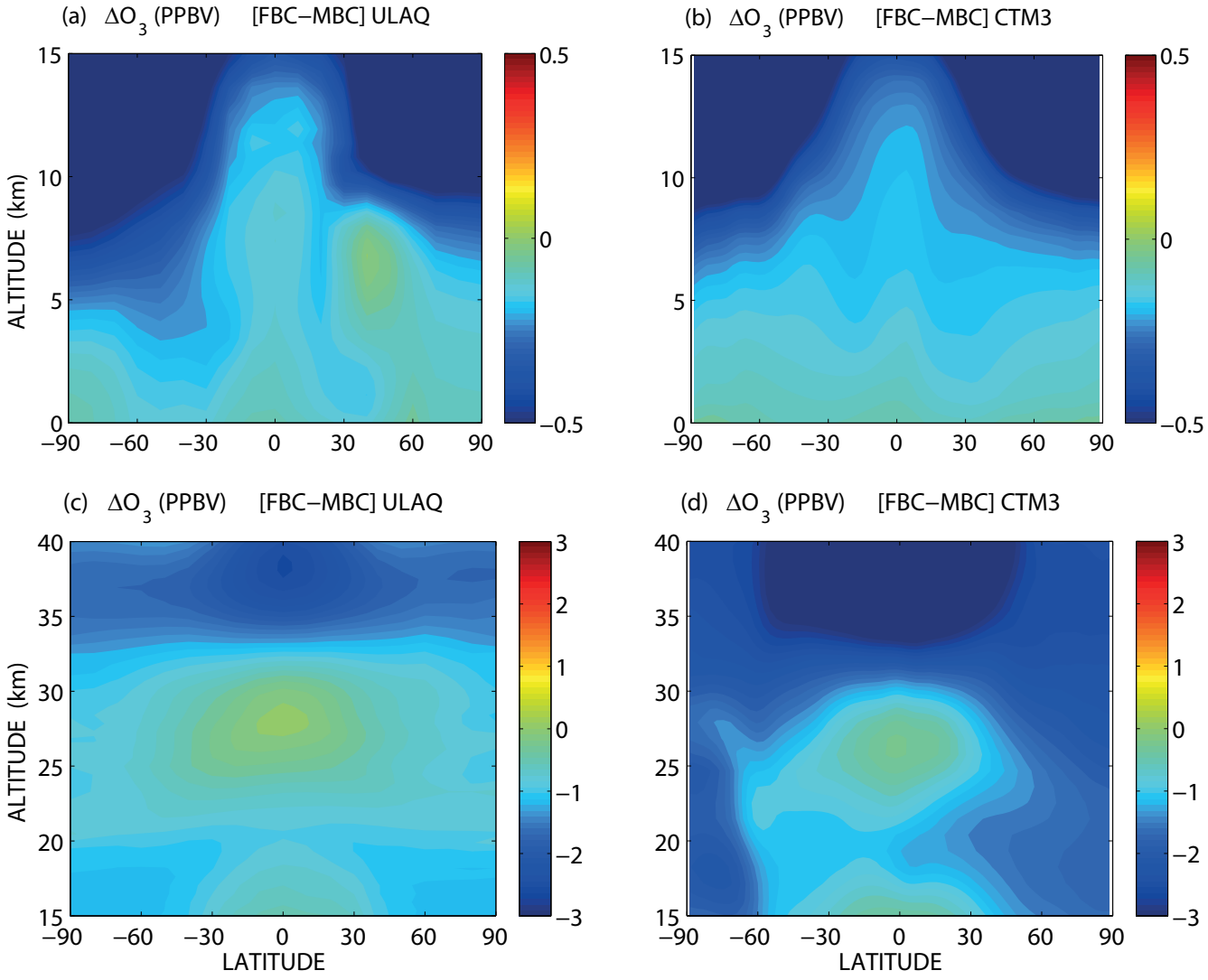

Figure 14: Panels (a, b): Zonal and annual mean of long-term tropospheric O_3 mixing ratio changes (AE-NA) (ppbv), for FBC-MBC results of ULAQ-CTM and Oslo-CTM3 respectively. Panels (c, d) are as in (a, b), but for the long-term stratospheric O_3 mixing ratio changes.

the indirect forcing, due to the low dust hygroscopicity (Bauer et al., 2007). The aerosol components from Table 3a produced a net RF decrease of $-5.7\,mW/m^2$ for the MBC case and $-6.1\,mW/m^2$ for the FBC case. An assessment of the indirect NO_x-induced aerosol change was made in Brasseur et al. (2015). Differences with respect to our calculations may arise in the treatment of the indirect effects related to aerosol-cloud interactions and in the feedbacks of aviation SO_x and NO_x emissions, whereas we have isolated the effects of NO_x emissions in the AE simulation. Here the calculated NO_x impact on sulfate aerosols is only due to aviation NO_x induced changes in the concentration of SO_2 oxidants.

4.4 Spatial RF distribution

From the modeling results, the net effects of aircraft NO_x emissions (short- and long-term) is then approximately zero on a global scale, with a small negative residual from different contributions (*i.e.*, cooling). This is visible in Fig. 16a and 16b, where the mean zonal RF values are shown separately for the O_3 short-term "instantaneous" value (MBC) and the different long-term responses (*i.e.*, CH_4, stratospheric H_2O, tropospheric and stratospheric O_3). The net forcing shows a clear positive peak at the northern mid-latitudes, where the largest change of O_3 column was produced by the aircraft emitted NO_x. As a result of the long CH_4 lifetime, the negative long-term responses of CH_4, H_2O and O_3 are spread globally in a quasi-uniform way and this produced an average cooling effect of approximately $-10\,mW/m^2$ over the tropics and in the Southern Hemisphere.

The geographical distribution of the long-term contributions discussed above (CH_4, stratospheric H_2O, O_3), are presented in Fig. 17. The net NO_x-related RF was dominated by the O_3 short-term peak at the northern hemisphere (see Fig. 16) and by the CH_4 cooling over the tropics and the southern hemisphere. Peak values of the CH_4 RF are located in the tropical region where there is the largest temperature difference of the surface and cloud layers with respect to the tropopause.

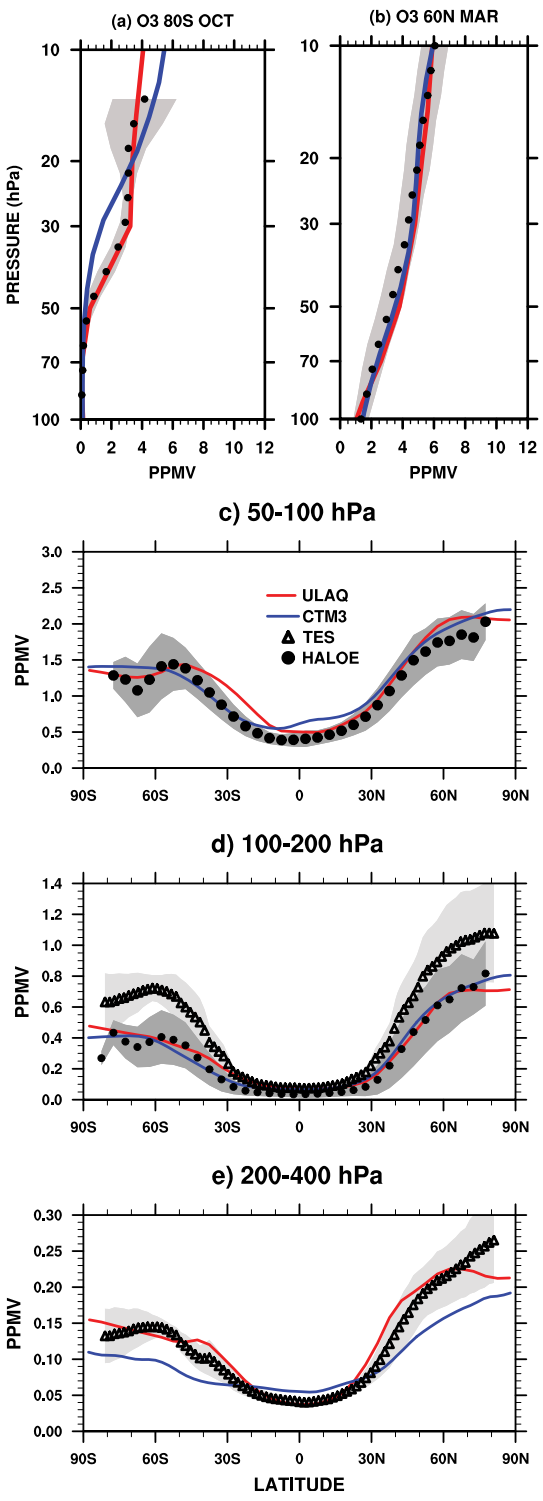

Figure 15: Stratospheric and tropospheric O_3 evaluation, using observations from HALOE (Grooss and Russell, 2005) and TES/Aura Level 3 ozone monthly data obtained from the NASA Langley Research Center (http://reverb.echo.nasa.gov/reverb/). Panels (a, b) show springtime polar vertical profiles from 10 to 100 hPa at 80S (October) and 60N (March), respectively. Panels (c to e) show annual mean latitudinal sections at pressure layers (c) 50–100 hPa, (d) 100–200 hPa and (e) 200–400 hPa. The grey areas show $\pm 1\sigma$ of the climatological zonal mean values (averaged over the years 1991–2005 for HALOE, and 2005–2012 for TES/Aura). Units are ppmv.

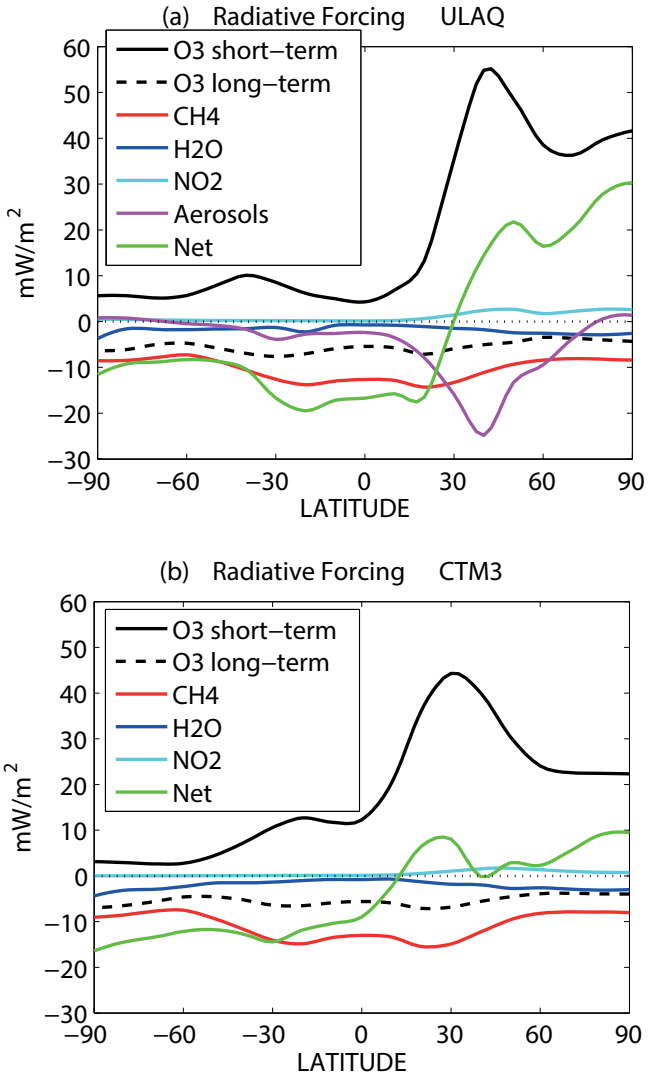

Figure 16: Annually and zonally averaged tropopause RF values due to aircraft NO_x emissions (AE-NA) shown by species in mW/m^2 for (a) ULAQ-CTM and (b) Oslo-CTM3 results. RF calculated with the ULAQ radiative transfer model, includes stratospheric temperature adjustment and total sky conditions. Short-, long-term effects (MBC and FBC-MBC, respectively) are presented separately for the O_3 RF. The net RF in panel (b) for the Oslo-CTM3 includes the aerosol contribution calculated by the ULAQ-CTM. The CH_4 curves includes also the RF due to CO_2 from CH_4 oxidation, on a 50 year time horizon.

Fig. 17 shows that the stratospheric long-term response of H_2O and O_3 is a cooling with maxima of approximately -2 mW/m^2 in the extra-tropics. The latitudinal gradient of the H_2O RF is consistent with the mixing ratio changes presented in Fig. 9. This is caused by a combination of stratospheric transport and CH_4 oxidation into water vapor. The tropical minimum in the stratospheric O_3 long-term RF in Fig. 17 is consistent with the mixing ratio changes presented in Fig. 14. Below 25 km altitude the negative O_3 changes are larger in the extra-tropics, whereas the opposite is found above 30 km, where the UV radiative impact tends to dominate, producing a positive RF (also see Fig. 13). This positive forcing partially mitigates the negative RF in

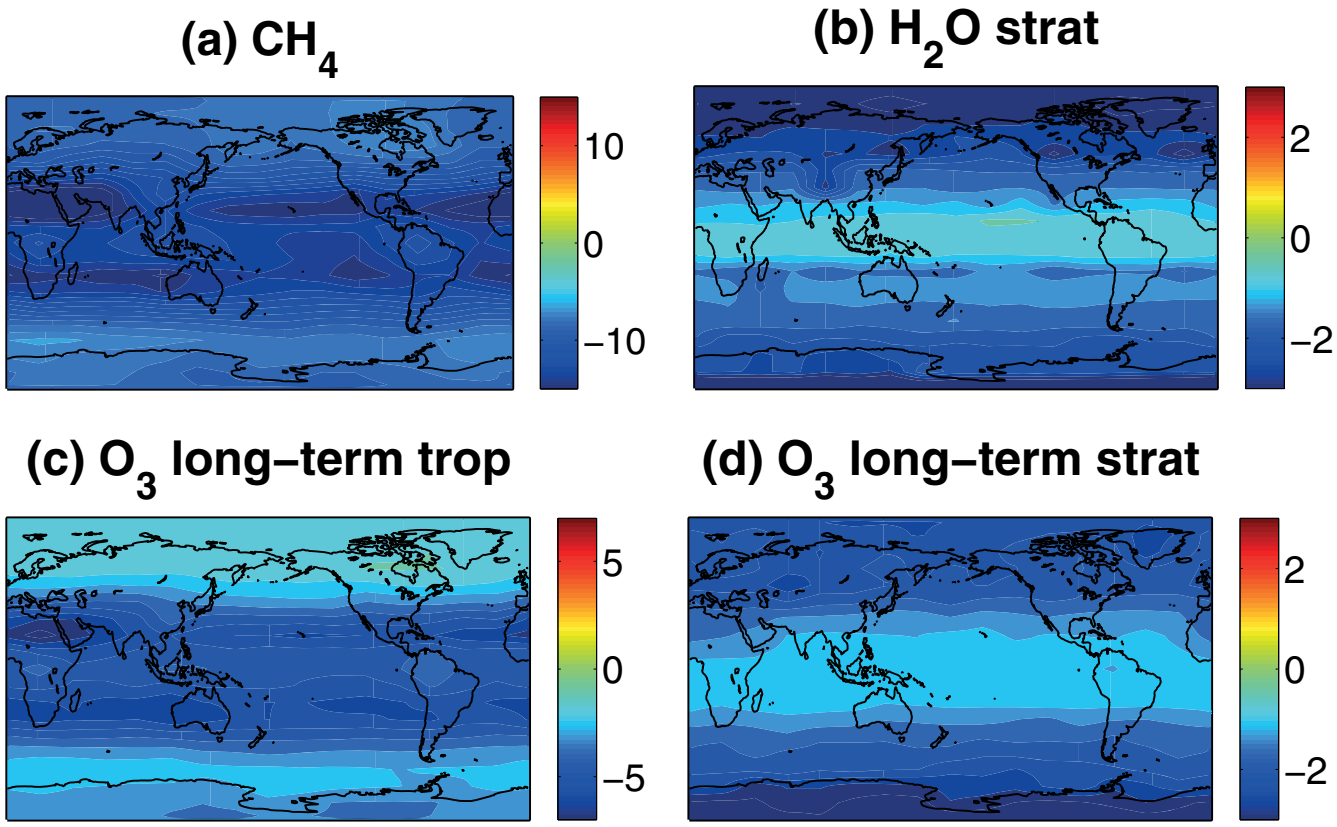

Figure 17: Annually averaged and temperature adjusted tropopause 2D RF values (mW/m^2) due to aircraft NO_x emissions (AE-NA) for (a) CH_4 (b) stratospheric H_2O (c) long-term tropospheric O_3 (FBC-MBC) and (d) long-term stratospheric O_3 (FBC-MBC). The CH_4 RF includes also the CO_2 contribution from CH_4 oxidation, on a 50 year time horizon.

the region where O_3 acts primarily as a greenhouse gas, *i.e.*, below ~ 25 km, where the largest stratospheric O_3 changes are found in the extra-tropics.

4.5 Aviation sulfate aerosols impact on NO_x chemistry

The tropospheric NO_x budget may be affected not only by direct aircraft emissions of NO_x, but also indirectly by aviation emissions of ultrafine sulfuric acid aerosols. The latter may significantly increase the available surface area density (SAD) for heterogeneous chemical reactions relevant for the NO_x-HNO_3 balance (Weisenstein et al., 1998; Danilin et al., 1998; Pitari et al., 2002a). Approximately 5 % of total emitted sulfur in aircraft plumes is ultrafine sulfuric acid particles (Curtius et al., 1998; Kärcher and Meilinger, 1998). These particles have the ability to greatly increase the sulfate aerosol SAD in the upper troposphere and lower stratosphere, thus mitigating the direct NO_x increase due to aircraft emissions, mainly via the hydrolysis of N_2O_5 and $BrONO_2$. Less NO_x increase results in less OH enhancement. This, in turn, means that there is less O_3 increase in the troposphere, leading to less CH_4 decrease (see Table 5). This also implies that the long-term stratospheric effects are slightly mitigated, *i.e.*, less H_2O decrease and less NO_x enhancement in the stratosphere and therefore, less stratospheric O_3 decrease when compared with the results presented in Table 3, where the sulfate aerosol SAD was kept unchanged by the aircraft emissions.

Nitrate aerosols tend to be more abundant for a more efficient NO_x conversion into HNO_3 on the enhanced sulfate SAD. However, the mass density and optical depth of sulfate and organic aerosols will be lowered if there is a decreased amount of oxidants (OH, H_2O_2, O_3, NO_3), which is due to the enhanced NO_x loss (see Table 5). According to the models, in this aerosol-sensitive case the net contribution to RF from aircraft NO_x emissions resulted in −6.2 mW/m^2, with an additional contribution of −0.5 mW/m^2 due to the effects of heterogeneous chemistry of NO_x on aviation sulfate SAD.

5 Conclusions

Two independent chemistry-transport models with troposphere-stratosphere coupling have been used to quantify the different radiative forcing components from NO_x aircraft emissions, by taking into account both the short-term tropospheric O_3 response and the long-term responses due to OH-driven changes of tropospheric CH_4 and then, in tropospheric HO_x chemistry and stratospheric H_2O, and finally on stratospheric O_3. A broad-band radiative transfer model has been applied offline, to calculate the tropopause adjusted RF from the perturbed greenhouse gases (*i.e.*, O_3, CH_4 and H_2O), as

well as from NO_2 absorption of UV-A, indirect SO_4 and SOA increase due to the tropospheric enhancement of oxidants (OH, H_2O_2, O_3, NO_3) and additional NO_3 aerosol formation from NO_x and HNO_3. Background chemistry results, where possible, are compared with measurements data and in general, the models are consistent with observations in their range of variability.

In the first case, the established experimental method of using a fixed mixing ratio boundary condition (MBC) was used. The model-average short-term O_3 and CH_4 RFs was 17.3 (24 mW/m^2/Tg-N) and −8.0 mW/m^2 (−11 mW/m^2/Tg-N) respectively. These are within the range of Holmes et al. (2011), Myhre et al. (2011) and Brasseur et al. (2015), which took into account inter-model differences. For completeness, simplified parametric formulations for long-term O_3 and stratospheric H_2O (Søvde et al., 2014; Pitari et al., 2015) were also included to derive respective RFs of −4.0 mW/m^2 (−5.6 mW/m^2/Tg-N) and −1.2 mW/m^2 (−1.7 mW/m^2/Tg-N). The long-term O_3 value is also consistent with the range of values published in Holmes et al. (2011) and Myhre et al. (2011) and for both perturbations in Khodayari et al. (2015). In the second case, a more computationally expensive experimental method that used a surface flux boundary condition (FBC) was conducted. Here, we were able to explicitly calculate the long-term effects from aviation NO_x emissions, without using simplified formulations. We found that the FBC experiment produced a CH_4 RF of −9.4 mW/m^2 (−13 mW/m^2/Tg-N) that is ∼ 17 % larger in absolute magnitude than the MBC estimate, while the long-term changes in O_3 and stratospheric H_2O were ∼ 29 % (−5.1 mW/m^2 or −7.2 mW/m^2/Tg-N) and ∼ 16 % (−1.4 mW/m^2 or −2.0 mW/m^2/Tg-N) larger in absolute magnitude respectively. The negative RF estimates are larger in terms of magnitude, and this is due to the compounding effects of the larger CH_4 lifetime changes (in absolute terms) and the corresponding radiative transfer calculations. In terms of the CH_4 lifetime estimates, the feedback factor of 1.4 largely compensated the differences in the simplified MBC formulation. However, using the actual CH_4 mixing ratio change in the radiative transfer calculation increases the absolute value of CH_4 RF estimate by ∼ 17 %. This is consistent with the findings of Myhre et al. (1998). In addition, the radiative balance is also affected by the decreasing amount of CO_2 produced at the end of the CH_4 oxidation chain: an average CO_2 accumulation change of −2.2 ppbv/yr is calculated with the models on a 50 year time horizon, with a corresponding RF=-1.6 mW/m^2. The FBC experiment also allows the long-term O_3 changes to be split between the tropospheric and stratospheric components, with the tropospheric effect contributing ∼ 75 % of the long-term O_3 RF (−3.9 mW/m^2).

The comparison between the FBC and MBC results in this study highlight that firstly, the long-term aviation NO_x impacts that have been reported in previous studies such as Holmes et al. (2011), Myhre et al. (2011), Søvde et al. (2014), Brasseur et al. (2015), are likely to be underestimated. Secondly, it is important to recognize that the underestimation of CH_4 RF, in absolute terms, will have a subsequent effect on the long-term O_3 and stratospheric water vapor estimate, which are derived from CH_4 RF in the simplified formulation. The underestimation found in the study was ∼ 17 %. Combining the short-term O_3 and long-term effects from CH_4, this study shows a RF decrease of more than 90 % in the magnitude of that calculated using simplified formulations. However, it should be noted that there is a trade-off in terms of computing time between the parameterizations (MBC) and using the explicit FBC method to calculate the long-term aviation NO_x effects. This study provides a revised estimate on the potential uncertainty that may arise when the MBC experiment is used in a CTM to simulate aviation NO_x effects.

Other contributions to net NO_x RF that have not been included in previous studies are those due to NO_2 absorption of UV-A (+0.6 mW/m^2) and aerosol perturbations; the latter were calculated only in the ULAQ model (−6.1 mW/m^2). In absolute terms, the resulting net RF related to aircraft NO_x emissions is calculated to be a small negative residual (−5.7 mW/m^2), with −6.2 mW/m^2 and −5.1 mW/m^2 in ULAQ and Oslo models respectively. This net negative RF residual is calculated to increase up to −6.2 mW/m^2 when the effects on NO_x chemistry due to the enhancement of the sulfate aerosol SAD produced by aviation emissions of SO_2 and SO_4 are also included.

Another multi model inter-comparison study of the aviation emissions impact on atmospheric ozone and methane (Olsen et al., 2013) did not show a model agreement comparable to ours. The main reason for this is that the seven models presented by Olsen et al. (2013) used a very different representation of chemistry and physics among them. Only three of these models were 3D offline models (*i.e.*, CTMs as our case), with the others being fully coupled climate chemistry models or a 2D earth system model. The three CTMs, however, did show a rather compact response to the aviation emissions, as in our study.

The results presented in this paper are important to the aviation community by providing a more robust and complete estimate of the likely effects from aircraft NO_x emissions, which accounts for the short- and long-term gaseous and aerosol impacts, with explicit CTM and RTM calculations. This study suggests that the net overall NO_x-related RF is smaller than previous estimates, and if we include the NO_x-aerosol effects as well, then the net RF is negative. Previous focus on the positive short-term O_3 effects should be extended to include not only the long-term contributions related to CH_4 but also, the indirect aerosols due to NO_x-chemistry. This has the wider implication that it may be the case that except for CO_2 and contrail/contrail-cirrus, which are known to produce significant globally-averaged warming effects,

the other aircraft RFs may produce a very small warming or even a cooling effect. However, further work is necessary to account for possible CTM and RTM model differences using a FBC setup and the effects of aerosols on NO_x chemistry. This is because an accurate quantitative measure of the net RF related to aviation NO_x is difficult for several reasons, as the uncertainties in lightning NO_x, HO_x-NO_x chemical kinetics, non-linearity among different NO_x sources, perturbation versus tagging approach, steady state versus transient emissions approach, treatment of future NO_x emissions, uncertainties in the treatment of complex aerosol-cloud interactions. So we conclude that a safe overall conclusion of the present study is that the net RF due to aviation NO_x emissions, considering both short- and long-term effects, might be very small and possibly also on the negative side.

Acknowledgements.

The authors acknowledge funding of the European Commission REACT4C project, under Grant No. ACP8-GA-2009-233772. TES/Aura data were obtained from the NASA Langley Research Center Atmospheric Science Data Center.

References

Andrews, A.E., K.A. Boering, B.C. Daube, S.C. Wofsy, M. Loewenstein, H. Jost, J.R. Podolske, C.R. Webster, R.L. Herman, D.C. Scott et al., 2001: Mean ages of stratospheric air derived from in situ observations of CO_2, CH_4, and N_2O. – J. Geophys. Res. **106**, 32295–32314.

Anderson, J., J.M. Russell III, S. Solomon, L.E. Deaver, 2000: Halogen Occultation Experiment confirmation of stratospheric chlorine decreases in accordance with the Montreal Protocol. – J. Geophys. Res. **105**, 4483–4490.

Austin, J., H. Struthers, J. Scinocca, D.A. Plummer, H. Akiyoshi, A.J.G. Baumgaertner, S. Bekki, G.E. Bodeker, P. Braesicke, C. Brühl et al., 2010: Chemistry-climate model simulations of spring Antarctic ozone. – J. Geophys. Res. **115**, D00M11 DOI: 10.1029/2009JD013577.

Ayres, B.R., H.M. Allen, D.C. Draper, S.S. Brown, R.J. Wild, J.L. Jimenez, D.A. Day, P. Campuzano-Jost, W. Hu, J. de Gouw et al., 2015: Organic nitrate aerosol formation via NO_3 + biogenic volatile organic compounds in the southeastern United States. – Atmos. Chem. Phys. **15**, 13377–13392, DOI:10.5194/acp-15-13377-2015.

Bauer, S.E., M.I. Mishchenko, A.A. Lacis, S. Zhang, J. Perlwitz, S.M. Metzenger, 2007: Do sulfate and nitrate coatings on mineral dust have important effects on radiative properties and climate modeling? – J. Geophys. Res. 112; DOI: 10.1029/2005JD006977.

Bousquet, P., B. Ringeval, I. Pison, E.J. Dlugokencky, E.-G. Brunke, Carouge, C., F. Chevallier, A. Fortems-Cheiney, C. Frankenberg, D.A. Hauglustaine et al., 2011 : Source attribution of the changes in atmospheric methane for 2006–2008. – Atmos. Chem. Phys. **11**, 3689–3700 ; DOI:10.5194/acp-11-3689-2011.

Brasseur, G., M. Gupta, B.E. Anderson, S. Balasubramanian, S. Barrett, D. Duda, G. Fleming, P.M. Forster, J. Fuglestvedt, A. Gettelman et al., 2015: Impact of aviation on climate: FAA's Aviation Climate Change Research Initiative (ACCRI) Phase II. – Bull. Amer. Meteorol. Soc., online, DOI:10.1175/BAMS-D-13-00089.1.

Brunner, D., J. Staehelin, H.L. Rogers, M.O. Köhler, J.A. Pyle, D. Hauglustaine, L. Jourdain, T.K. Berntsen, M. Gauss, I.S.A. Isaksen, and other, 2005: An evaluation of the performance of chemistry transport models - part 2: detailed comparison with two selected campaigns. – Atmos. Chem. Phys. **5**, 107–129.

Cariolle, D., D. Caro, R. Paoli, D.A. Hauglustaine, B. Cuénot, A. Cozic, R. Paugam, 2009: Parameterization of plume chemistry into large-scale atmospheric models: Application to aircraft NOx emissions. – J. Geophys. Res. **114**, D19302; DOI:10.1029/2009JD011873.

Chipperfield, M., Q. Liang, L. Abraham, S. Bekki, P. Braesicke, S. Dhomse, G. Di Genova, E.L. Fleming, S. Hardiman, D. Iachetti et al., 2013: Chapter 5: Model Estimates of Lifetimes. – In: Ko, M.K.W, P.A. Newman, S. Reimann, S.E. Strahan (Eds.): Lifetimes of Stratospheric Ozone-Depleting Substances, Their Replacements, and Related Species. SPARC Report No. 6, WCRP-15/2013

Chipperfield, M., Q. Liang, L. Abraham, S. Bekki, P. Braesicke, S. Dhomse, G. Di Genova, E.L. Fleming, S. Hardiman, D. Iachetti et al., 2014: Multi-model estimates of atmospheric lifetimes of long-lived Ozone-Depleting Substances: Present and future. – J. Geophys. Res. **119**, 2555–2573; DOI:10.1002/2013JD021097.

Chou, M.-D., M.J. Suarez, X.-Z. Liang, M.M.-H. Yan, 2001: A thermal infrared radiation parameterization for atmospheric studies. – NASA/TM-2001-104606 **19**, pp. 55.

Curtius, J., B. Sierau, F. Arnold, R. Baumann, R. Busen, P. Schulte, U. Schumann, 1998: First direct sulfuric acid detection in the exhaust plume of a jet aircraft in flight. – Geophys. Res. Lett. **25**, 923–926.

Danilin, M.Y., D.W. Fahey, U. Schumann, M.J. Prather, J.E. Penner, M.K.W. Ko, D.K. Weisenstein, C.H. Jackman, G. Pitari, I. Koeler et al., 1998 : Aviation fuel tracer simulation: model intercomparison and implications. – Geophys. Res. Lett. **25**, 3947–3950.

EC-JRC/PBL, European Commission (EC), Joint Research Centre (JRC)/Netherlands Environmental Assessment Agency (PBL), 2011: Emission Database for Global Atmospheric Research (EDGAR), release version 4.0. – http://edgar.jrc.ec.europa.eu.

Emmons, L.K., D.A. Hauglustaine, J.-F. Müller, M.A. Carroll, G.P. Brasseur, D. Brunner, J. Staehelin, V. Thouret, A. Marenco, 2000: Data composites of airborne observations of tropospheric ozone and its precursors. – J. Geophys. Res. 105, 20497–20538; DOI: 10.1029/2000JD900232.

Eyring, V., N. Butchart, D.W. Waugh, H. Akiyoshi, J. Austin, S. Bekki, G.E. Bodeker, B.A. Boville, C. Bruhl, M.P. Chipperfield et al., 2006: Assessment of temperature, trace species, and ozone in chemistry-climate model simulation of the recent past. – J. Geophys. Res. **99**, 111, D22308; DOI:10.1029/2006JD007327.

Eyring, V., M. Righi, A. Lauer, M. Evaldsson, S. Wenzel, C. Jones, A. Anav, O. Andrews, I. Cionni, E.L. Davin, et al., 2016: ESMValTool (v1.0) – a community diagnostic and performance metrics tool for routine evaluation of Earth system models in CMIP. – Geosci. Model Dev., **9**, 1747–1802, DOI:10.5194/gmd-9-1747-2016.

Fuglestvedt, J., T. Berntsen, G. Myhre, K. Rypdal, R.B. Skeie, 2008: Climate forcing from the transport sectors. – PNAS **105**, 454–458; DOI:10.1073/pnas.0702958104.

Gottschaldt, K., C. Voigt, P. Jöckel, M. Righi, R. Deckert, S. Dietmüller, 2013: Global sensitivity of aviation NO_x effects to the HNO_3-forming channel of the HO_2 + NO reaction. – Atmos. Chem. Phys. **13**, 3003–3025; DOI: 10.5194/acp-13-3003-2013.

Grewe, V., D. Brunner, M. Dameris, J.L. Grenfell, R. Hein, D. Shindell, J. Staehlin, 2001: Origin and variability of upper tropospheric nitrogen oxides and ozone at northern mid-latitudes. – Atmos. Env. **35**, 3421–343.

Grewe, V., E. Tsati, P. Hoor, 2010: On the attribution of contributions of atmospheric trace gases to emissions in atmospheric model applications. – Geosci. Model Dev. **3**, 487–499; DOI: 10.5194/gmd-3-487-2010.

Grooss, J.-U., J.M. Russell III, 2005: Technical note: A stratospheric climatology for O_3, H_2O, CH_4, NOx, HCl and HF derived from HALOE measurements. – Atmos. Chem. Phys. **5**, 2797–2807; DOI:10.5194/acp-5-2797-2005.

Guenther, A., T. Karl, P. Harley, C. Wiedinmyer, P.I. Palmer, C. Geron, 2006: Estimates of global terrestrial isoprene emissions using MEGAN (Model of Emissions of Gases and Aerosols from Nature). – Atmos. Chem. Phys. **6**, 3181–3210; DOI:10.5194/acp-6-3181-2006.

Hall, T.M., D.W. Waugh, K.A. Boering, R.A. Plumb, 1999: Evaluation of transport in stratospheric models. - J. Geophys. Res. **104**, 1881–18840.

Holmes, C.D., Q. Tang, M.J. Prather, 2011: Uncertainties in climate assessment for the case of aviation NO. – P. Natl. Acad. Sci. USA **108**, 10997–11002; DOI: 10.1073/pnas.1101458108.

Holtslag, A.A.M., E.I.F. DeBruijn, H.L. Pan, 1990: A high resolution air mass transformation model for short-range weather forecasting. – Mon. Wea. Rev. **118**, 1561–1575; DOI: 10.1175/1520-0493(1990)118<1561:AHRAMT>2.0.CO;2.

Hoor, P., J. Borken-Kleefeld, D. Caro, O. Dessens, O. Endresen, M. Gauss, V. Grewe, D. Hauglustaine, I.S.A. Isaksen, P. Jockel et al., 2009: The impact of traffic emissions on atmospheric ozone and OH: results from QUANTIFY. – Atmos. Chem. Phys. **9**, 3113–3136.

Hough, A.M., C.E. Johnson, 1991: Modelling the role of nitrogen oxides, hydrocarbons and carbon monoxide in the global formation of tropospheric oxidants. – Atmos. Environ. **25A**, 1819–1835.

ICAO, 2013: International Civil Aviation Organization. – http://www.icao.int/environmental-protection/Pages/modelling-and-databases.aspx.

ICAO/CAEP, 2009: International civil aviation organization (icao) / committee on aviation environmental protection (caep), agenda item 4: Modeling and databases task force (modtf) goals assessment results. – ICAO/CAEP Working Paper, Steering Group Meeting, Salvador, Brazil, 22–26 June 2009.

IPCC, 1999: Aviation and the global atmosphere. Intergovernmental Panel on Climate Change. J. Penner J. et al. (Eds.): Cambridge University Press, Cambridge, UK.

IPCC, 2013. Climate change 2013: Chapter 6. The physical science basis. Stocker, T.F. et al. (Eds.). – Cambridge University Press, UK.

Kärcher, B., U. Lohmann, 2002: A parameterization of cirrus cloud formation: homogeneous freezing of supercooled aerosols. – J. Geophys. Res. **107**, 4010, DOI: 10.1029/2001JD000470.

Kärcher, B., S.K. Meilinger, 1998: Perturbation of the aerosol layer by aviation-produced aerosols: a parameterization of plume processes. – Geophys. Res. Lett. **25**, 4465–4468.

Khodayari, A., S.C. Olsen, D.J. Wuebbles, D.B. Phoenix, 2015: Aviation NO_x-induced CH_4 effect: Fixed mixing ratio boundary conditions versus flux boundary conditions. – Atmos. Environ., 113, 135–139, DOI:10.1016/j.atmosenv.2015.04.070.

Köhler, M.O., G. Rädel, O. Dessens, K.P. Shine, H.L. Rogers, O. Wild, J.A. Pyle, 2008: Impact of perturbations to nitrogen oxide emissions from global aviation. – J. Geophys. Res. **113**; D11305, DOI:10.1029/2007JD009140.

Köhler, M.O., G. Rädel, K.P. Shine, H.L. Rogers, J.A. Pyle, 2012: Latitudinal variation of the effect of aviation NOx emissions on atmospheric ozone and methane and related climate metrics. – Atmos. Env. **64**, 1–9.

Kraabøl, A.G., T.K. Berntsen, J.K. Sundet, F. Stordal, 2002: Impacts of NOx emissions from subsonic aircraft in a global three-dimensional chemistry transport model including plume processes. – J. Geophys. Res. **107**, 4655; DOI: 10.1029/2001JD001019.

Kvalevåg, M.M., G. Myhre, 2007: Human Impact on Direct and Diffuse Solar Radiation during the Industrial Era. – J. Climate. **20**, 4874–4883; DOI:10.1175/JCLI4277.1.

Lamarque, J.F., T.C. Bond, V. Eyring, C. Granier, A. Heil, Z. Klimont, D. Lee, C. Liousse, A. Mieville, B. Owen et al., 2010: Historical (1850–2000) gridded anthropogenic and biomass burning emissions of reactive gases and aerosols: methodology and application. – Atmos. Chem. Phys. **10**, 7017–7039.

Lee, D.S., B. Owen, C. Fichter, L.L. Lim, D. Dimitriu, 2005: Allocation of International Aviation Emissions from Scheduled Air Traffic-present Day and Historical. – Report to UK Department for Environment, Food and Rural Affairs, London.

Lee, D.S., D.W. Fahey, P.M. Forster, P.J. Newton, R.C.N. Wit, L.L. Lim, B. Owen, R. Sausen, 2009: Aviation and global climate change in the 21st century. – Atmos. Environ. **43**, 3520–3537.

Lee, D.S., G. Pitari, V. Grewe, K. Gierens, J. Penner, A. Petzold, M. Prather, U. Schumann, A. Bais, T. Berntsen et al., 2010: Transport impacts on atmosphere and climate: Aviation. – Atmos. Environ. **44**, 4678–4734.

Minschwaner, K., R.J. Salawitch, M.B. McElroy, 1993: Absorption of Solar Radiation by O_2: Implications for O_3 and Lifetimes of N_2O, $CFCl_3$, and CF_2Cl_2. – J. Geophys. Res. **98**, 10, 543–10,561: DOI:10.1029/93JD00223.

Morgenstern, O., M.A. Giorgetta, K. Shibata, V. Eyring, D.W. Waugh, T.G. Shepherd, H. Akiyoshi, J. Austin, A. Baumgärtner, S. Bekki et al., 2010: A review of CCMVal-2 models and simulations. – J. Geophys. Res. **115**, D00M02; DOI:10.1029/2009JD013728.

Myhre, G., E.J. Highwood, K.P. Shine, F. Stordal, 1998: New estimates of radiative forcing due to well mixed greenhouse gases. – Geophys. Res. Lett. **25**, 2715–2718.

Myhre, G., J.S. Nielsen, L. Gulstad, K.P. Shine, B. Rognerud, I.S.A. Isaksen, 2007: Radiative forcing due to stratospheric water vapour from CH4 oxidation. – Geophys. Res. Lett., **34**, L01807, DOI:10.1029/2006gl027472.

Myhre, G., K. Shine, G. Readel, M. Gauss, I. Isaksen, Q. Tang, M. Prather, J. Williams, P. van Velthoven, O. Dessens et al., 2011: Radiative forcing due to changes in ozone and methane caused by the transport sector. – Atmos. Env. **45**, 387–394.

Myhre, G., D. Shindell, F.-M. Bréon, W. Collins, J. Fuglestvedt, J. Huang, D. Koch, J.-F. Lamarque, D. Lee, B. Mendoza et al., 2013: Anthropogenic and natural radiative forcing. – In: Climate Change 2013: the Physical Science Basis. Contribution of Working Group I to the Fifth Assessment Report of the Intergovernmental Panel on Climate Change, Cambridge University Press: Cambridge, United Kingdom and New York, NY, USA.

Olsen, S.C., G.P. Brasseur, D.J. Wuebbles, S.R.H. Barrett, H. Dang, S.D. Eastham, M.Z. Jacobson, A. Khodayari, H. Selkirk, A. Sokolov, N. Unger et al., 2013: Comparison of model estimates of the effects of aviation emissions on

atmospheric ozone and methane. – Geophys. Res. Lett., 40, 6004–6009, DOI:10.1002/2013GL057660.

Ott, L.E., K.E. Pickering, G.L. Stenchikov, D.J. Allen, A.J. De Caria, B. Ridley, R.-F. Lin, S. Lang, W.K. Tao, 2010: Production of lightning NO_x and its vertical distribution calculated from three-dimensional cloud-scale chemical transport model simulations. – J. Geophys. Res. 115, D04301, DOI:10.1029/2009JD011880.

Owen, B., D.S. Lee, L.L. Lim, 2010: Flying into the Future: Aviation Emissions Scenarios to 2050. – Env. Sci. Technol. **44**, 2255–2260.

Pitari, G., E. Mancini, A. Bregman, 2002a: Climate forcing of subsonic aviation: indirect role of sulfate particles via heterogeneous chemistry. – Geophys. Res. Lett. **29**, 2057; DOI: 10.1029/2002GL015705.

Pitari, G., E. Mancini, V. Rizi, D.T. Shindell, 2002b: Impact of future climate and emission changes on stratospheric aerosols and ozone. – J. Atmos. Sci. **59**, 414–440.

Pitari, G., D. Iachetti, E. Mancini, V. Montanaro, N. De Luca, C. Marizy, O. Dessens, H. Rogers, J. Pyle, V. Grewe et al., 2008: Radiative forcing from particle emissions by future supersonic aircraft. – Atmos. Chem. Phys. **8**, 4069–4084.

Pitari, G., V. Aquila, B. Kravitz, A. Robock, S. Watanabe, I. Cionni, N. De Luca, G. Di Genova, E. Mancini, S. Tilmes, 2014: Stratospheric Ozone Response to Sulfate Geoengineering: Results from the Geoengineering Model Intercomparison Project (GeoMIP). – J. Geophys. Res. **119**, 2629–2653; DOI:10.1002/2013JD020566.

Pitari, G., D. Iachetti, G. Di Genova, N. De Luca, O.A. Søvde, Ø. Hodnebrog, D.S. Lee, L. Lim, 2015: Impact of coupled NO_x/aerosol aircraft emissions on ozone photochemistry and radiative forcing. – Atmosphere **6**, 751–782; DOI:10.3390/atmos6060751, 2015.

Prather, M.J., D. Ehhalt, F. Dentener, R. Derwent, E. Dlugokencky, et al., 2001. Atmospheric chemistry and greenhouse gases. – In: Houghton, J.T. (Eds.): Climate Change 2001: The Scientific Basis, Contribution of Working Group I to the Third Assessment Report of the Intergovernmental Panel on Climate Change. – Cambridge University Press, Cambridge, United Kingdom and New York, NY, USA, 239–287.

Prather, M.J., X. Zhu, S.E. Strahan, S.D. Steenrod, J.M. Rodriguez, 2008: Quantifying errors in trace species transport modeling. – Proc. Natl. Acad. Sci. USA **105**, 19617—9621, DOI:10.1073/pnas.0806541106.

Ramaswamy, V., O. Boucher, J. Haigh, D. Hauglustaine, J. Haywood, G. Myhre, T. Nakajima, G.Y. Shi, S. Solomon et al., 2001: Radiative forcing of climate change. – In: Houghton, J.T. (Ed.): Climate Change 2001. – Cambridge Univ. Press, New York, 349–416.

Randles, C.A., S. Kinne, G. Myhre, M. Schulz, P. Stier, J. Fischer, L. Doppler, E. Highwood, C. Ryder, B. Harris et al., 2013: Intercomparison of shortwave radiative transfer schemes in global aerosol modeling: Results from the AeroCom Radiative Transfer Code Experiment. – Atmos. Chem. Phys. **13**, 2347–2379; DOI:10.5194/acp-13-2347-2013.

Rogers, H., H. Teyssedre, G. Pitari, V. Grewe, P. Van Velthoven, J. Sundet, 2002: Model intercomparison of the transport of aircraft-like emissions from sub- and supersonic aircraft. –Meteorol. Z. **11**, 151–159.

Sander, S.P., et al., 2011: Chemical Kinetics and Photochemical Data for Use in Atmospheric Studies, Evaluation No. 17. – Tech. Rep. **10-06**, Jet Propulsion Laboratory, Pasadena, California Institute of Technology, http://jpldataeval.jpl.nasa.gov/.

Schumann, U., H. Schlager, F. Arnold, J. Ovarlez, H. Kelder, Ø. Hov, G. Hayman, I.S. A. Isaksen, J. Staehelin, P.D. Whitefield, 2000: Pollution from aircraft emissions in the North Atlantic flight corridor: Overview on the POLINAT projects Model intercomparison of the transport of aircraft-like emissions from sub- and supersonic aircraft. – J. Geophys. Res. **105**, 3605–3631; DOI: 10.1029/1999jd900941.

Simos, D., 2008: PIANO User's Guide Version 5.0. – Lissys Limited, UK, 2008, www.piano.aero.

Skowron, A.M., D.S. Lee, J. Hurley, 2009: Aviation NO_x Global Warming Potential. - 2nd International Conference on Transport, Atmosphere and Climate, 25–28 June 2009, Aachen/Maastricht, Germany/Netherlands.

Skowron, A.M., 2013: The impact of emissions of nitrogen oxides from aviation on tropospheric chemistry – the counterbalancing roles of ozone and methane. – PHD thesis, Manchester Metropolitan University.

Søvde, O.A., M.J. Prather, I.S.A. Isaksen, T.K. Berntsen, F. Stordal, X. Zhu, C.D. Holmes, J. Hsu, 2012: The chemical transport model Oslo CTM3. – Geosci. Model Dev. **5**, 1441–469, DOI:10.5194/gmd-5-1441-2012.

Søvde, O.A., S. Matthes, A. Skowron, D. Iachetti, L. Lim, L., Ø. Hodnebrog, G. Di Genova, G. Pitari, D.S. Lee, G. Myhre, I.S.A. Isaksen, 2014: Aircraft emission mitigation by changing route altitude: A multi-model estimate of aircraft NO_x emission impact on O_3 photochemistry. – Atmos. Environ.; DOI:10.1016/j.atmosenv.2014.06.049.

Spivakovsky, C.M., J.A. Logan, S.A. Montzka, Y.J. Balkanski, M. Foreman-Fowler, D.B.J. Jones, L.W. Horowitz, A.C. Fusco, C.A.M. Brenninkmeijer, M.J. Prather et al., 2000: Three-dimensional climatological distribution of tropospheric OH: Update and evaluation. – J. Geophys. Res. **105**, 8931–8980; DOI:10.1029/1999JD901006.

Strahan, S.E., A.R. Douglass, R.S. Stolarski, H. Akiyoshi, S. Bekki, P. Braesicke, N. Butchart, M.P. Chipperfield, D. Cugnet, S. Dhomse et al., 2011: Using transport diagnostics to understand Chemistry Climate Model ozone simulations. – J. Geophys. Res. **116**, D17302; DOI: 10.1029/2010JD015360.

Unger, N., 2011: Global climate impact of civil aviation for standard and desulfurized jet fuel. – Geophys. Res. Lett. **38**, L20803; DOI:10.1029/2011GL049289.

van der Werf, G.R., J.T. Randerson, L. Giglio, G.J. Collatz, M. Mu, P.S. Kasibhatla, D.C. Morton, R.S. DeFries, Y. Jin, T.T. van Leeuwen, 2010: Global fire emissions and the contribution of deforestation, savanna, forest, agricultural, and peat fires (1997–2009). – Atmos. Chem. Phys. **10**, 11707–11735, DOI:10.5194/acp-10-11707-2010.

Waugh, D., T. Hall, 2002: Age of stratospheric air: Theory, observations, and models. – Rev. Geophys. **40**, 1010; DOI: 10.1029/2000RG000101.

Wecht, K.J., D.J. Jacob, C. Frankenberg, Z. Jiang, D.R. Blake, 2014: Mapping of North American methane emissions with high spatial resolution by inversion of SCIAMACHY satellite data. – J. Geophys. Res. **119**, 7741–7756; DOI:10.1002/2014JD021551.

Weisenstein, D., M. Ko, I. Dyominov, G. Pitari, L. Ricciardulli, G. Visconti, S. Bekki, 1998: The effects of sulfur emissions from HSCT aircraft: a 2-D model intercomparison. – J. Geophys. Res. **103**, 1527–1547.

Wild, O., M.J. Prather, H. Akimoto, 2001: Indirect long-term radiative cooling from NOx emissions. – Geophys. Res. Lett. **28**, 1719–1722; DOI:10.1029/2000gl012573.

Worden, J., S. Kulawik, C. Frankenberg, V. Payne, K. Bowman, K. Cady-Peirara, K. Wecht, J.-E. Lee, D. Noone, 2012: Profiles of CH_4, HDO, H_2O, and N_2O with improved lower tropospheric vertical resolution from Aura TES radiances. – Atmos. Meas. Tech. **5**, 397–411; DOI: 10.5194/amt-5-397-2012.